

## **A Regime Shift on Weddell Sea Continental Shelves with Local and Remote Physical and Biogeochemical Implications is Avoidable in a 2°C Scenario**

CARA NISSEN<sup>1</sup>, RALPH TIMMERMANN<sup>1</sup>, MARIO HOPPEMA<sup>1</sup>, AND JUDITH HAUCK<sup>1</sup>

<sup>1</sup> *Alfred Wegener Institute, Helmholtz Zentrum für Polar- und Meeresforschung, Bremerhaven, Germany*

(Manuscript received 14 December 2022, in final form 6 June 2023, accepted 6 June 2023)

**ABSTRACT:** Tipping points in the Earth system describe critical thresholds beyond which a single component, part of the system, or the system as a whole changes from one stable state to another. In the present-day Southern Ocean, the Weddell Sea constitutes an important dense-water formation site, associated with efficient deep-ocean carbon and oxygen transfer and low ice-shelf basal melt rates. Here, a regime shift will occur when continental shelves are continuously flushed with warm, oxygen-poor offshore waters from intermediate depth, leading to less efficient deep-ocean carbon and oxygen transfer and higher ice-shelf basal melt rates. We use a global ocean–biogeochemistry model including ice-shelf cavities and an eddy-permitting grid in the southern Weddell Sea to address the susceptibility of this region to such a system change for four twenty-first-century emission scenarios. Assessing the projected changes in shelf–open-ocean density gradients, bottom-water properties, and on-shelf heat transport, our results indicate that the Weddell Sea undergoes a regime shift by 2100 in the highest-emission scenario, SSP5–8.5, but not yet in the lower-emission scenarios. The regime shift is imminent by 2100 in the scenarios SSP3–7.0 and SSP2–4.5, but avoidable under the lowest-emission scenario SSP1–2.6. While shelf–bottom waters freshen and acidify everywhere, bottom waters in the Filchner Trough undergo accelerated warming and deoxygenation following the system change, with implications for local ecosystems and ice-shelf basal melt. Additionally, deep-ocean carbon and oxygen transfer decline, implying that the local changes ultimately affect ocean circulation, climate, and ecosystems globally.


**KEYWORDS:** Ocean; Continental shelf/slope; Southern Ocean; Carbon cycle; Climate change; Ocean models


### 1. Introduction

A tipping point can generally be defined as the critical threshold when a system qualitatively and rapidly changes its state in response to gradual or abrupt environmental change (Scheffer et al. 2001; Heinze et al. 2021); the subsequent regime shift involves immediate changes in system properties. More specifically, in climate sciences, the crossing of tipping points affects the global or regional climate and as such often entails far-reaching, negative consequences for societies (Pörtner et al. 2019). In this case, the full impact of the crossing of the tipping point can take centuries or more to unravel (Lenton et al. 2008, 2019; Heinze et al. 2021). Sometimes the crossing of a single tipping point can trigger the crossing of another one (Lenton et al. 2019; Rocha et al. 2018), illustrating why such a state change often has limited reversibility (Lenton et al. 2008; Heinze et al. 2021).

In the Southern Ocean, two examples of climate-relevant tipping points have been proposed, which both involve continental shelf processes (Lenton et al. 2008). As an undisputed example for a tipping point in the Southern Hemisphere, marine ice sheet instability could lead to an accelerating and irreversible loss of grounded ice on multidecadal or longer time scales (Oppenheimer 1998). The complete disintegration of the West Antarctic Ice Sheet, which mainly drains into the Ross Sea, the Amundsen Sea, and the Weddell Sea (Mercer 1968, 1978; Oppenheimer 1998), would lead to a global sea level rise of ~3.2 m (Bamber et al. 2009). While the observed ice-shelf basal melt rates in the Amundsen Sea have accelerated over the recent past (Rignot et al. 2019), implying that a tipping point might have already been crossed (Pörtner et al. 2019; Rosier et al. 2021), basal melt rates in the southern Weddell Sea are still low today, which is likely linked to low on-shelf flow of warm waters from the open ocean (Rignot et al. 2013, 2019).

As a second example, a shutdown of Antarctic Bottom Water (AABW) formation due to altered buoyancy fluxes on the Antarctic continental shelf and the associated shutdown or reduction in deep-ocean heat and carbon sequestration would directly impact global ocean circulation and climate on centennial to millennial time scales (Jacobs 2004; Marinov et al. 2006; Nissen et al. 2022). Simultaneously, given its importance in deep-ocean ventilation (Gordon 2001), a shutdown of bottom-water renewal would reduce the amount of oxygen available to benthic ecosystems both locally (immediate) and downstream (decades and longer) of the AABW formation sites (Matear et al. 2000; Frölicher et al. 2020). While its impacts would surely be far-reaching, two characteristics of a shutdown of AABW formation cause an ongoing debate on whether it constitutes a true example of a climate-relevant

 Denotes content that is immediately available upon publication as open access.

 Supplemental information related to this paper is available at the Journals Online website: <https://doi.org/10.1175/JCLI-D-22-0926.s1>.

Cara Nissen's current affiliation: Department of Atmospheric and Oceanic Sciences and Institute of Arctic and Alpine Research, University of Colorado, Boulder, Colorado.

*Corresponding author:* Cara Nissen, [cara.nissen@colorado.edu](mailto:cara.nissen@colorado.edu)

DOI: 10.1175/JCLI-D-22-0926.1

© 2023 American Meteorological Society. This published article is licensed under the terms of the default AMS reuse license. For information regarding reuse of this content and general copyright information, consult the AMS Copyright Policy ([www.ametsoc.org/PUBSReuseLicenses](http://www.ametsoc.org/PUBSReuseLicenses)).

tipping point or rather a regime shift: 1) the state change might take place gradually rather than rapidly and 2) the new state would only be transiently stable, given that AABW formation might eventually be reinvigorated once the forcing is abated or reversed (Lenton et al. 2008). Despite its global importance, the susceptibility of the Weddell Sea to the crossing of critical thresholds in ice-shelf basal melt rates, AABW formation, carbon sequestration, and deep-ocean oxygenation under different scenarios of future environmental change is not yet fully understood.

Presently, the southern Weddell Sea constitutes an important AABW formation region (Jacobs 2004; Meredith 2013; Morrison et al. 2020; Akhoudas et al. 2021), efficiently drawing down carbon to the deep ocean (Huhn et al. 2013; van Heuven et al. 2014). Recently, using simulations with a global ocean–biogeochemistry model, Nissen et al. (2022) have demonstrated that for a high-emission scenario, carbon sequestration with newly formed Weddell Sea dense waters, which descend the southern Weddell Sea continental slope to form AABW, is drastically attenuated by the year 2100. The authors attributed the attenuation to the freshening and warming of water masses on the southern continental shelves, which lowered their density and prevented newly formed dense waters from efficiently transporting carbon to depths  $> 2000$  m. While it remained an open question whether this finding was unique to the high-emission scenario, the increasing decoupling between bottom waters on the Weddell Sea continental shelves and in the open ocean (i.e., an increasing difference in their density) mainly controlled the simulated reduction in local deep-ocean carbon accumulation.

In general, the degree of shelf–open-ocean coupling differs across shelf regions around Antarctica, and the strength of the coupling can be characterized by the strength of the Antarctic Slope Front (ASF; Jacobs 1991; Thompson et al. 2018), that is, by the cross-shelf break gradient in, for example, subsurface temperature, oxygen, or density (Fig. 1). The ASF is weak in relatively warm shelf regions such as the Amundsen Sea, and the comparatively high bottom temperatures on the continental shelf are the result of frequent on-shelf transport of warm, oxygen-depleted Circumpolar Deep Water (CDW; see Figs. 1b–d herein; Thompson et al. 2018; Holland et al. 2019; Morrison et al. 2020). In comparison, the ASF is stronger in fresh shelf regions such as the eastern Weddell Sea (Figs. 1k–m) and in regions of dense water formation such as the northwestern and especially the southern Weddell Sea (Figs. 1e–j). Here, cold, dense waters on the continental shelves act as a subsurface barrier for the on-shelf transport of Warm Deep Water (WDW), the Weddell Sea version of CDW (Fahrbach et al. 1994; Thompson et al. 2018; Vernet et al. 2019). In the vicinity of the Filchner Trough in the southwestern Weddell Sea, which constitutes the main transport pathway of newly formed dense waters to the abyss (Foldvik et al. 1985; Darelius and Sallée 2018), some WDW enters the shelf seasonally (Årthun et al. 2012; Ryan et al. 2017, 2020), but this WDW only occasionally reaches the ice-shelf front today (Darelius et al. 2016). Overall, this explains the lower present-day ice-shelf basal melt rates in dense shelf regions compared to warm shelf regions (Rignot et al. 2013, 2019) and demonstrates the need to constrain the potential future changes in Weddell Sea shelf–open-ocean coupling, the

on-shelf transport of WDW, the export of newly formed dense waters from the shelves, and the associated deep-ocean carbon and oxygen transfer.

Hellmer et al. (2017) suggested that in the southern Weddell Sea, a tipping point is crossed as soon as the ASF is weakened enough so that the WDW is continuously flushed onto the continental shelves and into the ice-shelf cavity, which would then quickly accelerate ice-shelf basal melt. Based on the recent idealized modeling work by Daae et al. (2020), Bull et al. (2021), and Haid et al. (2022), whose model experiments were designed to force the system change, a preconditioning of waters both on the shelf (freshening and warming) and offshore (changes in winds and in the properties of the WDW core) is needed for this to occur. For the end of the twenty-first century, all existing model projections suggest enhanced Weddell Sea ice-shelf basal melt, but the expected increase ranges from less than twofold to over 15-fold compared to present-day rates (Hellmer et al. 2012; Timmermann and Hellmer 2013; Hellmer et al. 2017; Timmermann and Goeller 2017; Naughten et al. 2019, 2021; Nissen et al. 2022), which can be attributed to differences in, for example, the forcing scenario applied, the grid resolution of the respective model setup, and differences in the representation of ice shelf and seafloor topography. In particular, model resolution has recently been shown to impact the strength of the ASF, thereby controlling whether freshwater input, such as from ice-shelf basal melt, propagates to the open ocean or is retained on the continental shelves (Lockwood et al. 2021). This, in turn, directly impacts the susceptibility of the southern Weddell Sea to a possible system change under anthropogenic forcing. While even under the highest-emission scenario more recent projections with ocean-only models generally suggest a more moderate increase in ice-shelf basal melt (Naughten et al. 2019, 2021; Nissen et al. 2022) than those in earlier studies (see, e.g., Hellmer et al. 2012), uncertainty remains as to whether critical thresholds could be crossed in the Weddell Sea already by the end of this century.

Here, using the same global ocean–biogeochemistry model as in Nissen et al. (2022), which includes ice-shelf cavities and has an eddy-permitting grid resolution on the Weddell Sea continental shelves, we assess the possibility for a regime shift in the southern Weddell Sea under shared socioeconomic pathways (SSP forcing scenarios) until the end of the twenty-first century. In particular, we employ several different metrics to assess whether critical thresholds in shelf–open-ocean density differences, on-shelf transport of WDW, dense-water export from the continental shelves, and deep-ocean carbon sequestration have been crossed in the southern Weddell Sea by 2100. In addition to the high-emission scenario SSP5–8.5 assessed in Nissen et al. (2022), we here assess three lower-emission scenarios (SSP3–7.0, SSP2–4.5, and SSP1–2.6) to quantify the sensitivity of our findings to the chosen emission trajectory and expand the analysis to also include the ecosystem stressors oxygen and pH.

## 2. Methods

### a. Model simulations with FESOM-REcoM

We perform model experiments with the same setup as in Nissen et al. (2022). In particular, we use the global Finite

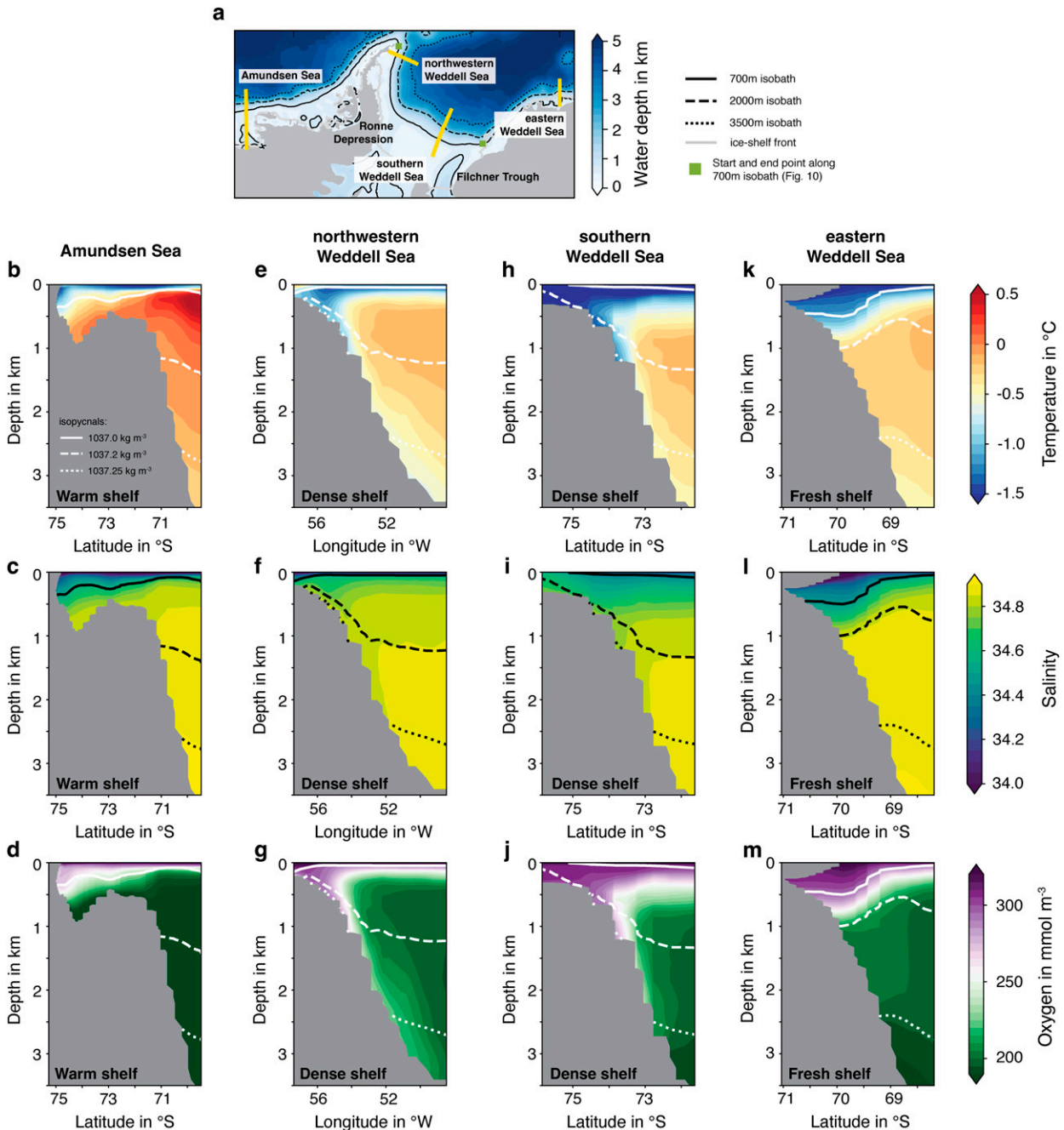


FIG. 1. Characterization of Antarctic continental shelf types (Thompson et al. 2018), including (a) the exact location of the transects (yellow lines): (b)–(d) The Amundsen Sea as an example of a warm shelf, (e)–(j) the northwestern and southern Weddell Sea as examples of dense shelves, and (k)–(m) the eastern Weddell Sea as an example of a fresh shelf. Colors depict the average distribution of (top) temperature, (middle) salinity, and (bottom) oxygen averaged over the 1990s of the historical FESOM-REcoM simulation assessed in this study (see section 2). White contours denote selected isopycnals of the potential density referenced to 2000 dbar, namely,  $1037.0 \text{ kg m}^{-3}$  (solid),  $1037.2 \text{ kg m}^{-3}$  (dashed), and  $1037.25 \text{ kg m}^{-3}$  (dotted). In (a), the Filchner Trough is marked, the ice-shelf front is indicated by the gray contour, and black contours denote the 700 m (solid), 2000 m (dotted), and 3500 m isobath (dashed). Green squares depict the start and end points of the transect shown in Fig. 10.

Element Sea ice Ocean Model (FESOM) version 1.4 (Wang et al. 2014). Its dynamic–thermodynamic sea ice model and its ice-shelf component are described in Danilov et al. (2015) and Timmermann et al. (2012), respectively. The Regulated Ecosystem Model

(REcoM) version 2 (Hauck et al. 2013; Karakus et al. 2021) resolves the biogeochemical cycles of carbon, nitrogen, silicon, iron, and oxygen and is coupled to FESOM for this study. The “total deep-ocean carbon inventory” referred to in section 3 is

composed of dissolved inorganic carbon, dissolved organic carbon, two types of sinking particulate organic carbon, sinking particulate inorganic carbon, particulate organic carbon associated with the two phytoplankton (diatoms and small phytoplankton), and two zooplankton groups (small zooplankton and krill), and particulate inorganic carbon associated with the small phytoplankton group. The biological contribution to changes in the carbon inventory is computed from sinking particulate organic carbon, and the physical contribution is the residual between changes in the inventory and the biological contribution. We note that with this definition, any carbon that is not actively sinking is assigned to the physical contribution even if it was a sinking particle of biological origin at some depth above the deep-ocean volume of interest. All model simulations are run on a mesh with 99  $z$ -levels in the vertical and an eddy-permitting grid resolution on the southern Weddell Sea continental shelves ( $\sim 3$ – $10$  km). The grid resolution increases to  $\sim 80$  km in the northern Weddell Sea.

For this study, transient model experiments are performed for the time period 1950–2100. At the surface, all model simulations are forced with 3-hourly atmospheric output from the AWI Climate Model (AWI-CM), namely its contribution to phase 6 of the Coupled Model Intercomparison Project (CMIP6; Semmler et al. 2020). The model tracers are initialized with output from the AWI-CM (FESOM tracers) and with output of a simulation for the Regional Carbon Cycle Assessment and Processes 2 (RECCAP2) project (REcoM tracers; unpublished). The model experiments are forced with atmospheric output from the historical AWI-CM simulation for the period 1950–2014 and with output from four emission scenarios for 2015–2100: SSP1–2.6, SSP2–4.5, SSP3–7.0, and SSP5–8.5 (sorted from low-emission to high-emission). For the SSP3–7.0 scenario, output of five ensemble members is available for the AWI-CM (Semmler et al. 2020). Here, we use the first ensemble member to force our model experiment, whose projected warming of Weddell Sea air temperatures is the second least across all ensemble members of this emissions scenario [see the supplement of Nissen et al. (2022)]. Atmospheric  $\text{CO}_2$  levels are taken from Meinshausen et al. (2017) for the historical period and from O'Neill et al. (2016) for the emission scenarios. By 2100, atmospheric  $\text{CO}_2$  has increased to 446 ppm (SSP1–2.6), 603 ppm (SSP2–4.5), 867 ppm (SSP3–7.0), and 1135 ppm (SSP5–8.5) for the four emission scenarios (Fig. 2a). Across the scenarios, the average Weddell Sea air temperature in the year 2100 ranges from  $-8.9^\circ\text{C}$  (SSP1–2.6) to  $-5.3^\circ\text{C}$  (SSP5–8.5), corresponding to a warming between  $1.8^\circ$  and  $5.4^\circ\text{C}$  relative to the 1990s (not shown). To assess the model drift in the absence of climate change and rising atmospheric  $\text{CO}_2$  levels, we additionally perform a control simulation, for which atmospheric conditions of the years 1950 (atmospheric  $\text{CO}_2$ ; 312.82 ppm) and 1955 (all other variables; corresponding to normal-year conditions with respect to the phasing of the Southern Annular Mode and El Niño–Southern Oscillation in the AWI-CM data) are repeated. We note that the control simulation, the historical simulation, and the scenario simulation under the high-emission scenario SSP5–8.5 are identical to those in Nissen et al. (2022), and more detail on the model setup can be found therein.

## b. Metrics to identify a system change

We use several different approaches to assess whether the southern Weddell Sea undergoes a system change with the possible crossing of tipping points, which are outlined in more detail in the following.

### 1) CHARACTERIZING CONTINENTAL SHELVES BASED ON SHELF–OPEN-OCEAN DENSITY GRADIENTS

#### (i) Bottom density differences

Different types of continental shelves (i.e., warm, fresh, or dense shelves) show distinct differences in their shelf–open-ocean gradient of subsurface temperature, salinity, and hence density (see Fig. 1 herein and Thompson et al. 2018). In this context, the difference  $\Delta\rho^b$  between the bottom densities on the continental shelf ( $\rho^{b,cs}$ ) and in the open ocean ( $\rho^{b,oo}$ ) is a metric for the potential transfer of newly formed dense waters from the continental shelf to the abyss:

$$\Delta\rho^b = \rho^{b,cs} - \rho^{b,oo}. \quad (1)$$

A bottom density higher on the continental shelf than in the open ocean is a prerequisite for the transfer of newly formed dense waters to greater depths or all the way to the seafloor, and the deep-ocean transfer potential is expected to be high for dense shelves such as the southern Weddell Sea. Consequently, the disappearance of this potential for deep-ocean transfer of newly formed dense waters can be interpreted as a system change. For all model experiments, we calculate the bottom density difference between every model grid cell of the southern Weddell Sea continental shelf (south of the 700 m isobath) and the open ocean, with *open ocean* being defined as the model grid cell with a water depth  $\geq 3500$  m that is closest to the respective grid cell on the shelf. For all “bottom” quantities reported throughout the paper, “bottom” refers to the deepest available model grid cell at each location.

#### (ii) Horizontal density differences across the continental shelf break

In addition, for all model experiments, we calculate the horizontal density difference  $\Delta\rho^{700m}$  between locations at the continental shelf break ( $\rho^{700m,sb}$ ) and in the open ocean ( $\rho^{700m,oo}$ ), which we here define to be located along the 700 m isobath:

$$\Delta\rho^{700m} = \rho^{700m,sb} - \rho^{700m,oo}. \quad (2)$$

In contrast to shelf–open-ocean differences in bottom density [Eq. (1)], these horizontal density differences are more directly linked to the shelf–open-ocean exchange of WDW, which is generally limited in dense shelf regions due to the presence of dense waters on the continental shelf, resulting in a negative density difference (see Fig. 1 herein; Thompson et al. 2018; Haid et al. 2022). In general, the link between the horizontal density difference and the actual on-shelf flow of WDW can be expected to be stronger the shorter the distance is over which the density gradient is computed. Therefore, for this metric, we define the *open ocean* as the location with a water depth  $\geq 2000$  m that is closest to the respective grid cell at the shelf break. We note, however,

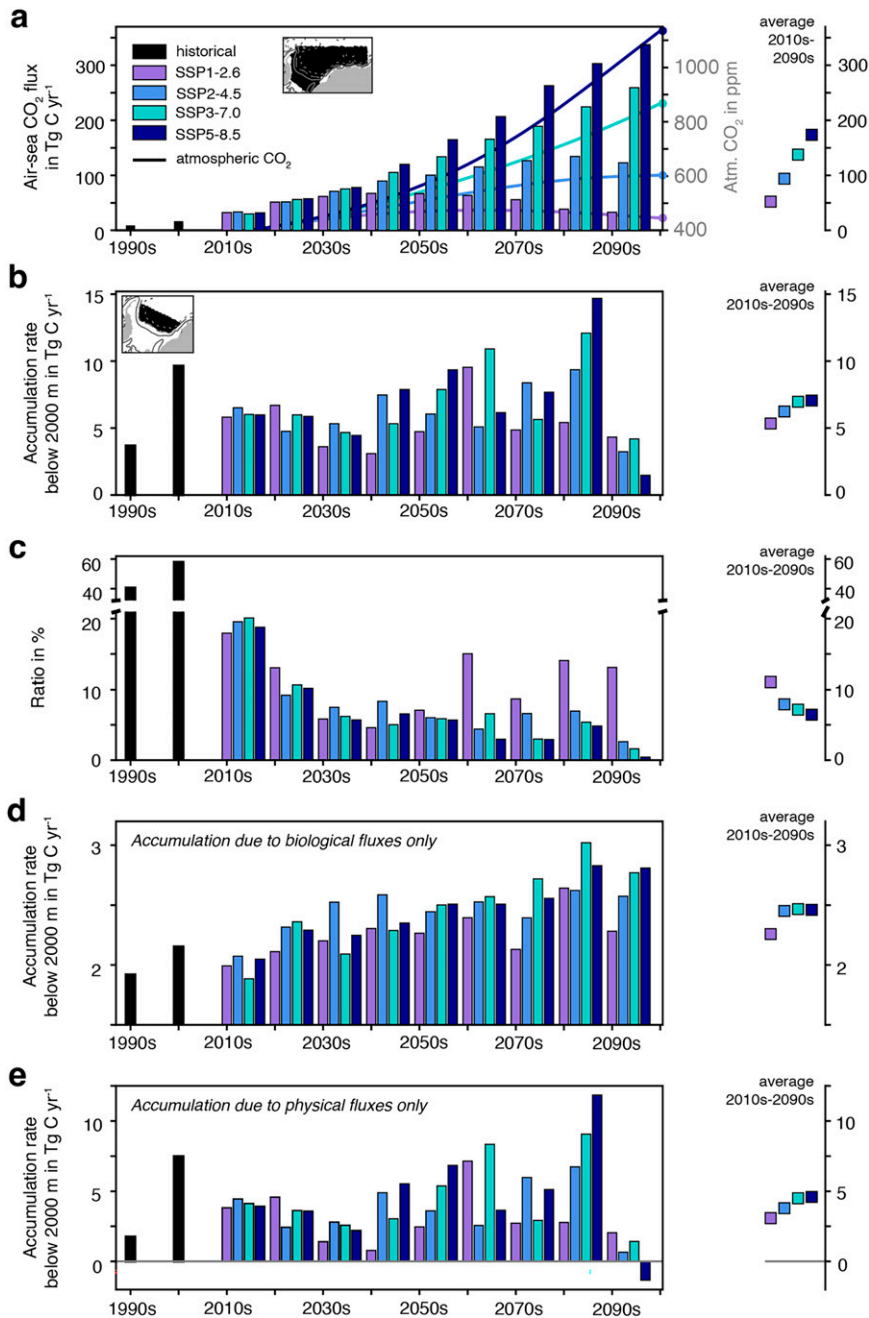


FIG. 2. (a) Air-sea  $\text{CO}_2$  flux (in  $\text{Tg C yr}^{-1}$ ) integrated over the Weddell Sea (see map) and averaged over each decade between the 1990s and the 2090s (left y axis). A positive flux denotes a flux into the ocean. Black bars denote the historical period, and colors from the 2010s onward show the different emission scenarios. The colored lines show the evolution of atmospheric  $\text{CO}_2$  in each scenario; circles highlight the level for the year 2100 (right y axis). The colored squares on the right correspond to the average air-sea  $\text{CO}_2$  flux between the 2010s and the 2090s for each emission scenario. (b) As in (a), but for the carbon accumulation rate below 2000 m in the southern Weddell Sea (see map). (c) The ratio (in %) between the deep-ocean carbon accumulation rate in (b) and the air-sea  $\text{CO}_2$  flux in (a). Note the broken y axis in (c). Also shown are the contributions of (d) biological and (e) physical fluxes to the total deep-ocean carbon accumulation in (b). The biological contribution to changes in the carbon inventory is computed from sinking particulate organic carbon, and the physical contribution is the residual between changes in the inventory and the biological contribution.

that qualitatively the results presented in section 3 are insensitive to this choice. Similar to the bottom-density differences, a reversal in the sign of the horizontal density gradient at 700 m over the twenty-first century can be interpreted as a system change, in which case the southern Weddell Sea would transition from a dense shelf to a warm shelf (Fig. 1).

## 2) CHANGEPOINT ANALYSIS TO SEPARATE GRADUAL FROM ABRUPT CHANGE

To assess whether bottom-water properties on the continental shelves change significantly between 1980 and 2100 in the different emission scenarios and to determine whether any change occurs gradually or includes abrupt changes, we apply the R package “Detection of Structural Changes in Climate and Environmental Time Series” to our model output (EnvCPT; Beaulieu and Killick 2018; Killick et al. 2021). We apply this methodology to the time series of annual mean bottom-density differences between the open ocean and the continental shelf sea [Eq. (1)] and bottom temperature, salinity, oxygen, and pH at each location on the southern continental shelves of the Weddell Sea. We calculate pH offline from monthly model output using the routines to model the ocean carbonate system (mocsy v2.0; Orr and Epitalon 2015). As in Nissen et al. (2022), we fit eight statistical models to the time series, of which four include changepoints (see our online supplemental material for model equations of each fit): (i), (ii) a constant mean with or without first-order autocorrelation, (iii), (iv) a constant linear trend with or without first-order autocorrelation, (v), (vi) a mean with changepoints with or without first-order autocorrelation, and (vii), (viii) a linear trend with changepoints with or without first-order autocorrelation. To identify the model that is best suited to describe the respective time series, the R package ranks all model fits using the Akaike information criterion (Akaike 1974). Here, we use a minimum segment length of 20 in the analysis, thereby requiring at least 20 years between any two changepoints detected. We note that the qualitative findings regarding the scenario differences are rather insensitive to this choice, while unsurprisingly, the exact timing of any changepoints identified and the exact statistics of any fit is sensitive to choosing a smaller or larger minimum segment length. For our application, we are mostly interested in long-term change in bottom-water properties and the presence or absence of abrupt changes in the mean or the slope of a given time series as an indicator for system change. In that context, we note that the presence of first-order autocorrelation in a time series affects year-to-year variability, but to a lesser extent long-term trends. Therefore, for the visualization of the results (see Figs. 6 and 7), we group the respective model fits with and without first-order autocorrelation together, allowing us to more clearly distinguish whether 1) a *mean*-model or a *trend*-model and 2) a model *with* or *without* changepoints best describes the model data.

## 3. Results

### a. Carbon transfer from the surface to the deep ocean across emission scenarios

Over the course of the twenty-first century, the simulated Weddell Sea air–sea CO<sub>2</sub> fluxes track the increase in atmospheric CO<sub>2</sub>

for each emission scenario (Fig. 2a). As a result, the oceanic sink of CO<sub>2</sub> in the Weddell Sea increases from 9.1 Tg C yr<sup>-1</sup> in the 1990s to 33 Tg C yr<sup>-1</sup> (SSP1–2.6), 123 Tg C yr<sup>-1</sup> (SSP2–4.5), 259 Tg C yr<sup>-1</sup> (SSP3–7.0), and 338 Tg C yr<sup>-1</sup> (SSP5–8.5) in the 2090s. While the CO<sub>2</sub> flux is highest in the high-emission scenario for each decade after the 2010s, the evolution of deep-ocean carbon-accumulation rates in the southern Weddell Sea is more variable in time and across emission scenarios (Fig. 2b). Acknowledging strong decadal variability, the rate in the lowest-emission scenario (SSP1–2.6) even exceeds the one in the highest-emission scenario (SSP5–8.5) in several decades, with deep-ocean carbon accumulation in, for example, the 2090s amounting to 4.3 and 1.5 Tg C yr<sup>-1</sup> in the SSP1–2.6 and SSP5–8.5 scenario, respectively.

The ratio of deep-ocean carbon accumulation and local surface-uptake of CO<sub>2</sub> provides a first-order insight into whether any trend in carbon accumulation in the upper ocean is translated into a corresponding trend in the deep ocean. Acknowledging that some of the carbon being sequestered in the deep ocean could be provided laterally from outside of the Weddell Sea as opposed to by local surface uptake of CO<sub>2</sub> (Hoppema et al. 2001), we here assume this lateral carbon transport to be relatively constant to first order. This ratio amounts to >40% in the historical simulation (black bars in Fig. 2c), but to only 0.5% in the 2090s for the SSP5–8.5 scenario, reflecting the attenuation in deep-ocean carbon accumulation discussed in more detail in Nissen et al. (2022). Notably, while there is some attenuation also for the scenarios SSP3–7.0 and SSP2–4.5 (although less than for SSP5–8.5), no attenuation in deep-ocean carbon accumulation is apparent in the SSP1–2.6 scenario when referencing to the scenario period. While the deep-ocean accumulation in the 2090s of this scenario (13% of the surface uptake) is lower than the ratios in the 1990s and 2000s, it exceeds the average ratio of 11% after the 2010s (Fig. 2c).

Any change in deep-ocean carbon accumulation is caused by changes in the downward transport of carbon through either biological or physical fluxes. In the model, for all emission scenarios, biological downward fluxes (i.e., the sinking of particulate organic carbon across 2000 m depth) generally steadily increase throughout the twenty-first century, namely from 1.9 Tg C yr<sup>-1</sup> in the 1990s (51% of the total accumulation) to 2.3 Tg C yr<sup>-1</sup> (53%; SSP1–2.6), 2.6 Tg C yr<sup>-1</sup> (81%; SSP2–4.5), and 2.8 Tg C yr<sup>-1</sup> (67% for SSP3–7.0 and 186% for SSP5–8.5) in the 2090s (Fig. 2d). Therefore, in none of the emission scenarios can these biological fluxes explain the simulated variability in deep-ocean carbon accumulation. Instead, the simulated evolution of the contribution of physical fluxes closely resembles that of the total deep-ocean carbon accumulation (cf. Figs. 2b,e). In fact, physical fluxes alone explain >99% of the simulated variability in deep-ocean carbon accumulation for each scenario (based on the linear correlation between the two annual mean time series). Due to this similarity between scenarios, it appears reasonable to assume that the main driver of the simulated attenuation in carbon sequestration for the SSP5–8.5 scenario discussed in Nissen et al. (2022), namely the increasing decoupling between bottom waters on the southern continental shelves and in the open ocean, also controls the simulated variability in all other

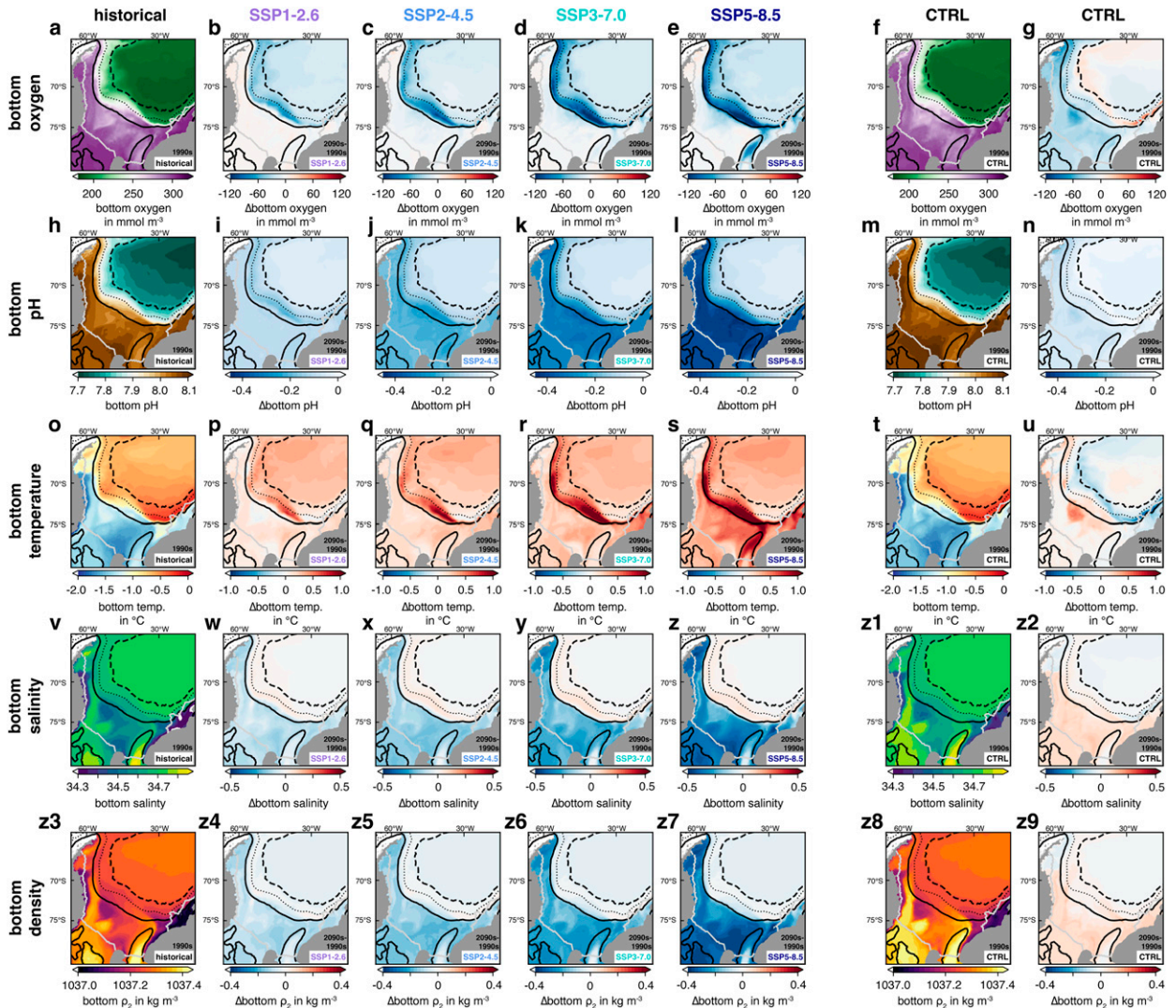


FIG. 3. Bottom oxygen concentrations (in  $\text{mmol m}^{-3}$ ) (a) in the 1990s and (b)–(e) in the 2090s relative to the 1990s for the different emission scenarios, sorted from the low-emission scenario SSP1–2.6 in (b) to the high-emission scenario SSP5–8.5 in (e). (f),(g) Bottom oxygen concentrations in the control simulation. (h)–(n),(o)–(u),(v)–(z2),(z3)–(z9) As in (a)–(g), but for bottom pH, bottom potential temperature (in  $^{\circ}\text{C}$ ), bottom practical salinity, and bottom potential density referenced to 2000 dbar (in  $\text{kg m}^{-3}$ ), respectively. In all panels, the ice-shelf front is shown as the gray contour, and black contours denote the 700 m (solid), 2000 m (dotted), and 3500 m (dashed).

scenarios, justifying the focus on this component for the remainder of section 3.

*b. Projected changes in dense-water transfer to the abyss based on bottom-water properties*

Bottom-water properties on the southern Weddell Sea continental shelves differ from those in the open ocean in the 1990s. Bottom oxygen and pH levels in the 1990s are highest on the continental shelves ( $>270 \text{ mmol m}^{-3}$  and  $>8.0$ ) and decline toward the deeper areas of the Weddell Sea ( $<190 \text{ mmol m}^{-3}$  and  $<7.8$  where it is deeper than 3500 m; Figs. 3a,h). This is unsurprising, as it reflects (i) the better mixed water column for shallower regions, where bottom

waters have more frequent exchange with the atmosphere, whereas the oxygen levels in deeper region result from mixing of these well-oxygenated shelf waters and relatively oxygen-poor WDW and (ii) the imprint of organic matter remineralization in the deeper regions (see also Nissen et al. 2022). While the simulated oxygen levels in the top  $\sim 2000$  m are in good agreement with observations (e.g., Hoppema 2004), we note that in contrast to observations, minimum open-ocean oxygen levels in the model are wrongly located below the WDW core (i.e., below  $\sim 2500$  m) rather than within its core for some shelf regions (see Figs. 1 and 3). This bias is the remainder of the initial adjustment of our simulation to the new model grid and atmospheric forcing (not shown), and deep-ocean

ventilation with AABW renewal continuously reduces the bias (for the Weddell Sea, see Fig. 3g). It should be noted that the full replenishment of the abyss with oxygen-rich waters takes much longer than our simulation time. Still, this kind of model bias likely only has a small effect on the results presented below, as the waters entering the southern Weddell Sea continental shelves mostly originate from the top 2500 m. In the 1990s, bottom waters on the continental shelves are on average  $\sim 1^\circ\text{C}$  colder than those in the open ocean (typically  $< -1.4^\circ$  and  $> -0.6^\circ\text{C}$  in the two regions, respectively; Fig. 3o). For bottom salinity and density, the model not only simulates differences between the continental shelf and the open ocean, but also suggests substantial spatial variability on the southern continental shelf itself (Figs. 3v,z). The simulated bottom salinity and density is highest close to the ice-shelf front in the Ronne Depression on the southwestern shelf and in the Filchner Trough (up to 34.8 and  $1037.4\text{ kg m}^{-3}$ , respectively), which is in general agreement with observations (Janout et al. 2021). We note, however, that there is disagreement between the model (Filchner Trough) and the observations (Ronne Depression) on where along the ice-shelf front the maximum bottom salinity is located.

Over the course of the twenty-first century, bottom waters in the model regionally undergo substantial deoxygenation, acidification, warming, and freshening. In the 2090s, the decline in bottom oxygen concentrations compared to the 1990s exceeds  $130\text{ mmol m}^{-3}$  along the southern continental slope for both the SSP3–7.0 and SSP5–8.5 scenario and locally amounts to up to  $116\text{ mmol m}^{-3}$  (SSP2–4.5) and  $86\text{ mmol m}^{-3}$  (SSP1–2.6) even in the two lower-emission scenarios (Figs. 3b–e). The decline on the continental shelves is much smaller in comparison and is only substantial in the Filchner Trough region in the SSP5–8.5 scenario, where the decline is locally  $>100\text{ mmol m}^{-3}$  (Fig. 3e). Interestingly, the pattern of the projected change in Weddell Sea bottom temperatures mirrors that of the oxygen changes (cf. Figs. 3p–s to Figs. 3b–e), illustrating the close link between these two variables (see also Fig. 1). Along the continental slope, bottom waters warm by up to  $0.8^\circ$ – $1.4^\circ\text{C}$  depending on the emission scenario (Figs. 3p–s), with the warming in the Filchner Trough only exceeding  $1^\circ\text{C}$  for the SSP5–8.5 scenario (up to  $1.3^\circ\text{C}$ ; Fig. 3s). In contrast to the patterns of deoxygenation and warming, the strongest acidification and freshening are not located along the continental slope, but on the southern continental shelves (Figs. 3i–l,w–z). The projected acidification is strongest between the ice-shelf front and the 700 m isobath for all scenarios, with the decline in bottom pH exceeding 0.4 for the SSP5–8.5 scenario. In contrast, the projected freshening is strongest close to the ice-shelf front, with bottom salinity declining by up to 0.19 (SSP1–2.6), 0.23 (SSP2–4.5), 0.38 (SSP3–7.0), and 0.47 (SSP5–8.5), while bottom salinity along the continental slope and in the open ocean even increases by up to 0.13 for the SSP5–8.5 scenario. On the continental shelves, both the projected reduction in sea ice growth in the area (up to  $-16\%$ ; Fig. 4a) and the projected increase in ice-shelf basal melt ( $+26\%$  to  $79\%$  across scenarios; Fig. 4b) contribute to the simulated freshening, explaining why its maximum is located there instead of farther offshore. Acknowledging that some of the projected changes are also seen in the control simulation, albeit smaller in magnitude (Figs. 3 and 4), bottom waters on the southern continental

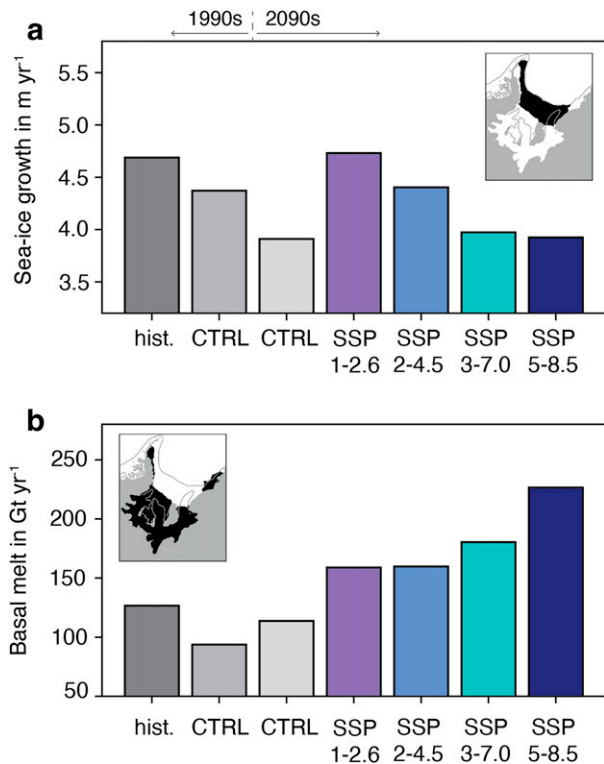


FIG. 4. (a) Average sea ice growth (in  $\text{m yr}^{-1}$ ) on the southern Weddell Sea continental shelves (see inset) in the 1990s in the historical simulation (dark gray), in the 1990s in the control simulation (gray), in the 2090s in the control simulation (light gray), and in the 2090s in the four emission scenarios (colors). (b) As in (a), but for the average ice-shelf basal melt (in  $\text{Gt yr}^{-1}$ ) in the southern Weddell Sea (see inset).

shelves overall shift to lighter densities as a result of both warming and freshening by the year 2100 for all emission scenarios, but in particular for the high-emission scenario SSP5–8.5.

The projected density reduction of bottom waters on the continental shelves directly impacts the potential for these waters to reach the deep ocean as they descend the continental slope during AABW formation, with the aforementioned consequences for carbon sequestration (Nissen et al. 2022). In the 1990s, bottom density on the continental shelves outside of the ice-shelf cavities exceeds that in the open ocean in the Ronne Depression and particularly in the Filchner Trough [red areas in Fig. 5a; see section 2b and Eq. (1)]. In these regions, the bottom density on the continental shelves is up to  $0.17\text{ kg m}^{-3}$  higher than in the open ocean, indicating a high potential of these waters to reach the abyss as part of AABW. As this distribution closely resembles that of bottom salinity on the continental shelves (see Fig. 3v), it is bottom salinity rather than temperature that appears to control this high potential for deep-ocean transfer. Acknowledging the model bias in the location of maximum bottom salinity (see above), the distribution is in general agreement with our observation-based understanding of the formation of dense shelf waters in the southern Weddell Sea, namely, high-salinity shelf water being formed during



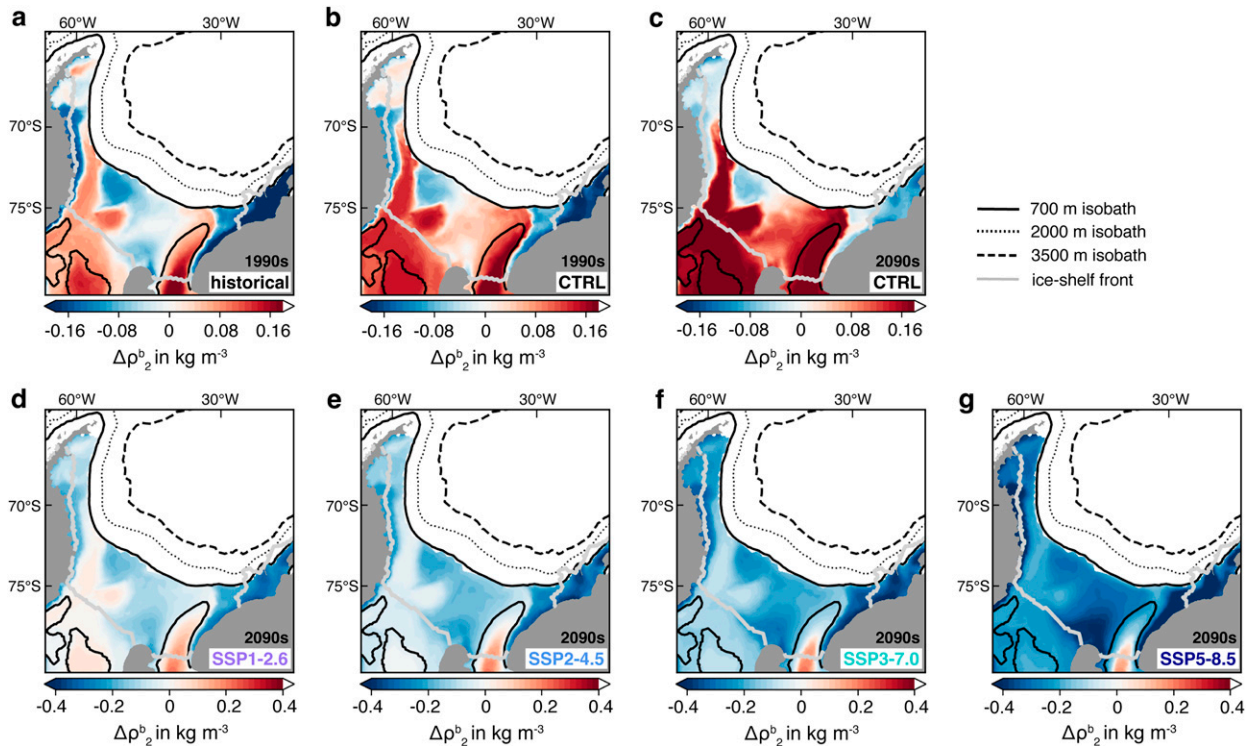


FIG. 5. (a) Difference in bottom potential density  $\rho_2$ , i.e., referenced to 2000 dbar (in  $\text{kg m}^{-3}$ ), between every location on the southern Weddell Sea continental shelves and the open ocean as a measure of the deep-ocean transfer potential [Eq. (1)]. Each location on the shelf is matched with the closest point with a water depth  $\geq 3500$  m in the open ocean to calculate the density difference. Red colors denote regions where the bottom density on the continental shelf exceeds that in the open ocean. (b),(c) As in (a), but for the 1990s and 2090s, respectively, of the control simulation. (d)–(g) As in (a), but for the 2090s of the four emission scenarios. In all panels, the ice-shelf front is shown as the gray contour, and black contours denote the 700 m (solid), 2000 m (dotted), and 3500 m (dashed) isobath. Note the difference in scale between (a)–(c) and (d)–(g).

sea ice formation close to Ronne Depression, which then flows via the ice-shelf cavity toward the Filchner Trough, where it exits the cavity as ice-shelf water and ultimately leaves the continental shelves (Foldvik et al. 1985). In contrast to the control simulation, for which these regions of high deep-ocean transfer potential strengthen over the course of the simulation (from  $\sim 0.1 \text{ kg m}^{-3}$  close to the 700 m isobath in the 1990s to  $>0.16 \text{ kg m}^{-3}$  in the 2090s; Figs. 5b,c), this potential decreases for all emission scenarios (Figs. 5d–g). In particular, in the 2090s, these regions of high deep-ocean transfer potential are absent for the SSP2–4.5, SSP3–7.0, and SSP5–8.5 scenarios (only blue colors close to the 700 m isobath in Figs. 5e–g) and are also reduced, but at least partly sustained for the SSP1–2.6 scenario (see red colors close to the 700 m isobath at Filchner Trough and close to Ronne Depression in Fig. 5d). This implies that apart from this lowest-emission scenario, bottom waters on the southern Weddell Sea continental shelves lose their ability to substantially contribute to AABW renewal by the end of the twenty-first century.

### c. Characterizing the change in bottom-water properties: Gradual or abrupt?

Whether the projected changes in bottom-water properties occur gradually or abruptly over the twenty-first century can provide insights into whether a system change takes place

(see section 2b). In general, for all bottom-water properties, a trend-model (i.e., a constant linear trend with or without changepoints and first-order autocorrelation) is best suited to describe the time series in most places (green colors in Fig. 6), but the fraction of the continental shelf area whose temporal evolution is best described by such a trend-model depends on the emission scenario. For example, for the shelf–open-ocean differences in bottom density, the fraction of the total shelf area occupied by a trend-model is smallest for the SSP1–2.6 and SSP2–4.5 scenarios ( $\sim 60\%$ ), while amounting to  $\sim 80\%$  for the higher-emission scenarios (Figs. 6a–d). Comparing the two highest-emission scenarios, a changepoint in the trend (light green) is identified more often for the SSP5–8.5 scenario than for the SSP3–7.0 scenario (39% vs 19% of the surface area; Figs. 6c,d). While this generally also holds for the other variables (Figs. 6e–t), the variables differ in some key aspects. Notably, for bottom pH and salinity, the model allowing for changepoints in the linear trend (light green) is almost exclusively identified as the best model for all scenarios (pH) and the SSP5–8.5 scenario (salinity), implying changes in the rate of acidification and freshening at least once throughout the century at almost every location on the continental shelves. For both bottom temperature and oxygen, the Filchner Trough stands out as a region for which a linear trend with changepoints best

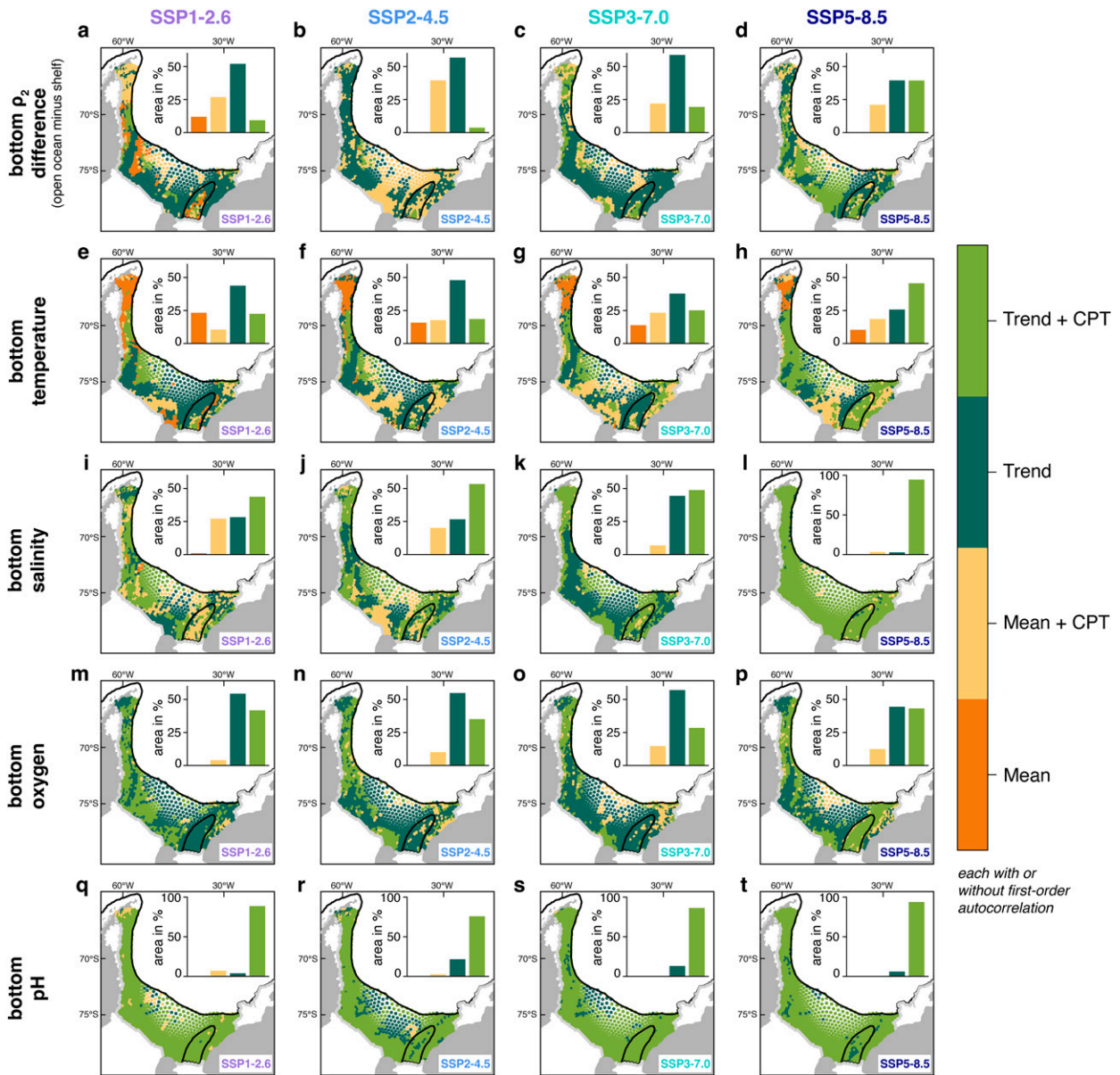


FIG. 6. Results of the changepoint analysis applied to the time series from 1980 to 2100 for each emission scenario of (a)–(d) the difference in bottom potential density  $\rho_2$  between the open ocean and each location on the southern continental shelves [Eq. (1)], (e)–(h) bottom potential temperature, (i)–(l) bottom practical salinity, (m)–(p) bottom oxygen concentrations, and (q)–(t) bottom pH (see also Figs. 3 and 5). In each panel, the color denotes the type of linear model that best describes the respective time series. The models are distinguished by whether a constant mean (orange) or a constant linear trend (green) best describes the data and by whether or not changepoints (CPT) are included (darker and lighter colors). Models with and without first-order autocorrelation are grouped together. See section 2b for details. The bar plot in each panel shows the relative shelf area covered by each model type. In all panels, the ice-shelf front is shown as the gray contour, and the black contour denotes the 700 m isobath.

describes the time series for the SSP5–8.5 scenario, while a model without changepoints is often identified as the best model for its surroundings (Figs. 6h,p; last changepoint typically between 2070 and 2080).

Quantitatively assessing the differences in the statistical fit between the time series with and without changepoints illustrates the significance of a changepoint being identified for

the rate of change of a given quantity. In general, for all five variables, trends at locations at which a changepoint is identified (light green in Fig. 6) are up to one order of magnitude larger than trends at locations with a constant trend throughout the simulation period (dark green in Fig. 6; compare y axes between the rows in Fig. 7; the trend after the last changepoint in the time series is considered). The change in

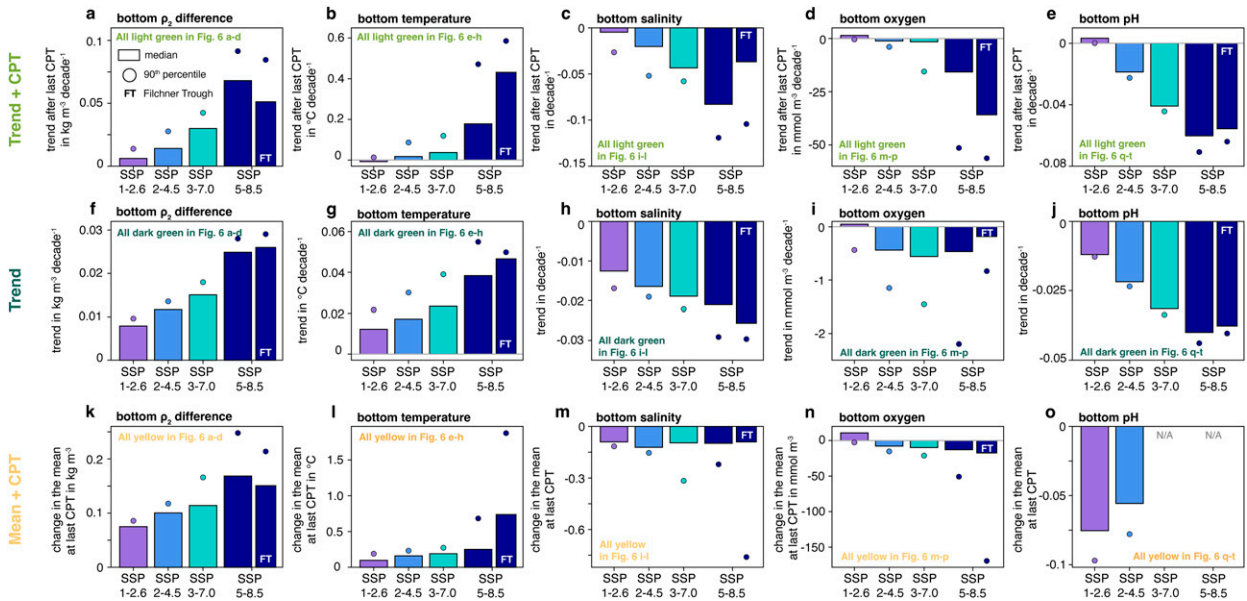


FIG. 7. (a)–(e) Median decadal trend in (a) the bottom density difference  $\rho_2$  (in  $\text{kg m}^{-3} \text{decade}^{-1}$ ) [see Eq. (1)], (b) bottom potential temperature (in  $^{\circ}\text{C decade}^{-1}$ ), (c) bottom practical salinity (in  $\text{decade}^{-1}$ ), (d) bottom oxygen concentrations (in  $\text{mmol m}^{-3} \text{decade}^{-1}$ ), and (e) bottom pH (in  $\text{decade}^{-1}$ ) after the last changepoint (CPT) identified for locations at which Trend+CPT (with or without autocorrelation) is best suited to describe the time series in each emission scenario (light green regions in Fig. 6). (f)–(j) As in (a)–(e), but for the locations at which (f)–(j) Trend (with or without autocorrelation) and (k)–(o) Mean+CPT (with or without autocorrelation) is best suited to describe the time series in each emission scenario (dark green and yellow regions in Fig. 6). For (k)–(o), the difference in the mean before and after the last CPT is shown. Note the up to one order of magnitude difference in the y-axis scale between the rows and that the area represented by each bar differs (see Fig. 6). Dots above each bar denote the 90th percentile. For the SSP5–8.5 scenario, results for the Filchner Trough region (FT; locations east of  $42^{\circ}\text{W}$ , deeper than 500 m, and outside of ice-shelf cavities) are shown separately next to the column for the full area.

the mean before and after the last CPT locally exceeds the decadal change for grid cells with a change in the linear trend (Figs. 7a–e vs Figs. 7k–o), but we acknowledge that the area covered by grid cells best described by a change in the mean throughout the time series generally amounts to  $<20\%$  (especially for higher-emission scenarios). Overall, this demonstrates that the presence of abrupt changes toward the end of a time series is a consequence of a stepwise change (Mean+CPT) or an acceleration of the change (Trend+CPT) in the respective property, with the latter resulting in substantially larger change if the accelerated trends are sustained for multiple decades. Unsurprisingly, across emission scenarios and variables, the projected change occurs fastest in the SSP5–8.5 scenario (Fig. 7). In particular, the median rates of bottom-density decoupling ( $+0.068 \text{ kg m}^{-3} \text{decade}^{-1}$ ), freshening ( $-0.083 \text{ decade}^{-1}$ ), and acidification ( $-0.06 \text{ decade}^{-1}$ ) are 46%–127% times higher in the SSP5–8.5 scenario than in the SSP3–7.0 scenario ( $+0.03 \text{ kg m}^{-3}$ ,  $-0.043$ , and  $-0.041 \text{ decade}^{-1}$ , respectively; Figs. 7a,c,e). After the last identified changepoint, bottom waters on the continental shelves warm at a rate of  $0.18^{\circ}\text{C decade}^{-1}$  in the highest-emission scenario, with the warming rate amounting to even  $0.47^{\circ}\text{C decade}^{-1}$  for the 90th percentile (Fig. 7b). At the same time, bottom waters deoxygenate at  $15.7 \text{ mmol m}^{-3} \text{decade}^{-1}$  (median), which corresponds to a 10 times faster deoxygenation for the SSP5–8.5 scenario than for the second-highest emission scenario SSP3–7.0 ( $1.56 \text{ mmol m}^{-3} \text{decade}^{-1}$ ; Fig. 7d). In the Filchner

Trough, bottom waters in SSP5–8.5 even warm at a rate of  $0.43^{\circ}\text{C}$  (median) and  $0.59^{\circ}\text{C}$  (90th percentile)  $\text{decade}^{-1}$ , while losing oxygen at a rate of  $35.9 \text{ mmol m}^{-3}$  (median) and  $56.3 \text{ mmol m}^{-3} \text{decade}^{-1}$  (90th percentile; Figs. 7b,d), making this region a hotspot of warming and deoxygenation in the highest-emission scenario.

#### d. The Filchner Trough as a hotspot of change

On a transect directly north of the Filchner Trough sill, simulated temperatures are below  $-1^{\circ}\text{C}$  throughout the water column in the 1990s (Fig. 8). Over the twenty-first century, annual mean temperatures at middepths exceed  $-1^{\circ}\text{C}$  for all scenarios for individual years from the 2020s onward, but the higher the emission scenario, the more frequent, the longer and the warmer these pulses of relatively warm water become over time (Figs. 8a–d; these waters are also oxygen-poor; see also Fig. 1). Remarkably, for the SSP5–8.5 scenario, temperatures below 400 m (and at the surface) increase to  $>-0.5^{\circ}\text{C}$  for all years after 2085 (Fig. 8d). Overall, comparing the 2090s to the 1990s, the bottom waters at the continental shelf break at Filchner Trough warm by up to  $1^{\circ}\text{C}$  (Fig. 8e) and deoxygenate by up to  $75 \text{ mmol m}^{-3}$  over the twenty-first century (Fig. 8f).

The projected warming for the 2090s translates into an enhanced on-shelf heat transport relative to the 1990s for all emission scenarios (Fig. 9). While the on-shelf heat transport in the

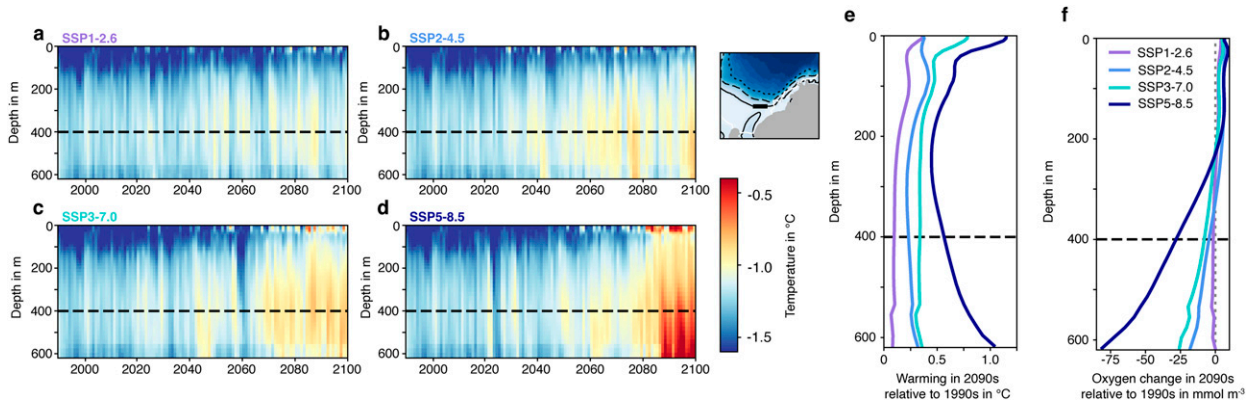


FIG. 8. (a)–(d) Evolution of the annual mean potential temperature (in  $^{\circ}\text{C}$ ) at the continental shelf break near the Filchner Trough sill (see map) as a function of depth and time for the four emission scenarios. (e) Profiles of temperature increase in the 2090s for each emission scenario relative to the 1990s. (f) As in (e), but for the change in oxygen concentrations (in  $\text{mmol m}^{-3}$ ). The horizontal dashed line in all panels highlights a depth of 400 m, below which the strongest warming occurs for the SSP5–8.5 scenario. The maximum depth of Filchner Trough sill is 555 m in our model.

control simulation declines over the whole water column from the 1990s to the 2090s (from  $5.55$  to  $4.61 \times 10^{19} \text{ J yr}^{-1}$ ; Fig. 9a), the heat transport for the SSP5–8.5 scenario is 225% larger in the 2090s than in the 1990s ( $20.23$  vs  $6.22 \times 10^{19} \text{ J yr}^{-1}$ ;  $21.86$  vs  $7.18 \times 10^{19} \text{ J yr}^{-1}$  or a 204% increase when using daily model output) and thereby exceeds the transport in all other scenarios ( $8.06$ – $13.28 \times 10^{19} \text{ J yr}^{-1}$ ) in the 2090s by far. The increase is driven by a combination of changes in the on-shelf volume transport (see gray dots in Fig. 9a) and the warming of waters at the continental shelf break (Fig. 8), with the latter causing the main part of the increase (difference between gray dots and bars in Fig. 9a). In agreement with the depth profile of warming over the twenty-first century (Fig. 8), the scenario differences in the on-shelf heat transport are especially pronounced for the lower half of the water column (Fig. 9b). Below 400 m, the on-shelf heat transport in the 2090s for the SSP5–8.5 scenario exceeds even that in the SSP3–7.0 scenario by almost a factor of two ( $4.54$  vs  $2.45 \times 10^{19} \text{ J yr}^{-1}$ ). Most notably, the on-shelf heat transport between 2098 and 2100 is 33% larger than the one in the 2090s for the highest-emission scenario (blue dots in Fig. 9b), further illustrating the pronounced and accelerating changes in this region at the very end of this simulation.

Assessing density differences at 700 m between the continental shelf break and the open ocean [section 2a; Eq. (2)], the Filchner Trough region shows clear characteristics of a dense shelf region in the 1990s (density at the continental shelf break exceeds that in the open ocean by  $>0.16 \text{ kg m}^{-3}$ ; dark red colors in Fig. 10). Given that the same is true for the shelf regions both in the northwestern Weddell Sea and in front of the Ronne Depression, this suggests that a strong ASF in most parts of the southwestern Weddell Sea prevents the continuous flushing of the continental shelves with WDW in the present-day (see also Fig. 1). Over the twenty-first century, the positive cross-shelf break density differences are first eroded and eventually change sign at Filchner Trough and Ronne Depression for all emission scenarios except SSP1–2.6 and even for all emission scenarios in the northwestern

Weddell Sea. In fact, by the year 2100, the density at 700 m in the open ocean is  $>0.16 \text{ kg m}^{-3}$  higher than the density at the continental shelf break in the highest-emission scenario (Fig. 10d). This reversal is almost entirely driven by the changes in density at the continental shelf break and on the shelves, as the density of the WDW core offshore only changes marginally (not shown). Overall, these changes in density structure at the continental shelf break and thus in the characteristics of the ASF are in line with the projected changes in on-shelf heat transport described above.

There is a particularly close correspondence between the cross-shelf break density gradient and the on-shelf heat transport when filtering out the interannual variability of these two metrics. Any change or variability in the former explains  $\geq 70\%$  of the variability in the latter on decadal or multidecadal time scales ( $R^2 \geq 0.7$  for the highest-emission scenarios; Figs. 11a,b). In the highest emission scenario SSP5–8.5, the on-shelf heat transport increases drastically after the density difference is continuously negative and amounts to  $\sim -0.1 \text{ kg m}^{-3}$  for multiple consecutive years (Fig. 11a; note the flipped y axis). While the density difference is also continuously negative in the last  $\sim 15$  years of the SSP3–7.0 scenario, its magnitude is lower ( $\sim -0.05 \text{ kg m}^{-3}$ ; Fig. 11b), implying that a positive density difference alone does not immediately result in a flushing of the continental shelves with WDW.

Putting the projected changes at the Filchner Trough across emission scenarios in relation to the projected atmospheric warming (Figs. 11c–e), only the SSP5–8.5 scenario projects a warming of up to  $6^{\circ}\text{C}$ , explaining the much stronger oceanic changes by the year 2100 in this scenario (Figs. 8–10). Notably, for an atmospheric warming of both  $4^{\circ}$  and  $5^{\circ}\text{C}$ , the different emission scenarios project rather similar changes in the cross-shelf break density differences (Fig. 11c), the on-shelf heat transport (Fig. 11d), and bottom temperature (Fig. 11e). This suggests that both the SSP3–7.0 and SSP2–4.5 scenarios are on the same trajectory as the SSP5–8.5 scenario, with drastic changes in the lower-emission scenarios possibly

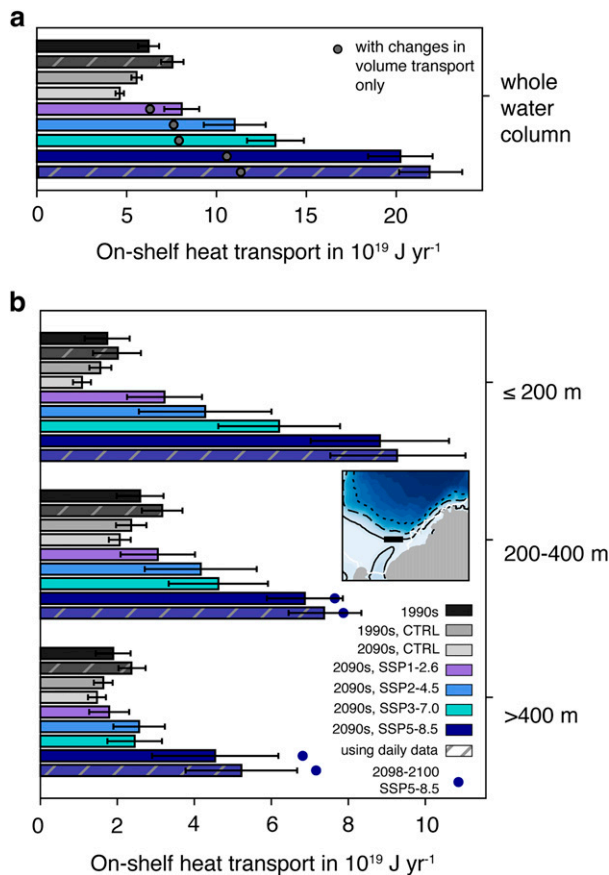


FIG. 9. Average on-shelf heat transport (in  $10^{21}\text{ J yr}^{-1}$ ) at Filchner Trough along the 700 m isobath (see map) calculated from monthly model output in the 1990s in the historical simulation (dark gray), in the 1990s in the control simulation (gray), in the 2090s in the control simulation (light gray) and in the 2090s in the four emission scenarios (colors). Hatched bars denote the on-shelf heat transport calculated from daily model output in the 1990s and 2090s for the SSP5–8.5 scenario (daily model output not available for other scenarios). The whiskers denote one standard deviation within each decade (based on annual mean values). Transports are integrated (a) over the whole water column and (b) within different depth intervals. In (a), the gray dots correspond to the on-shelf heat transport caused by the increase in volume transport only for each emission scenario, using monthly or daily climatological temperatures for the 1990s in the calculation. The contribution of warming to the increase in heat transport thus corresponds to the difference between the gray dot and each colored bar relative to the one in the 1990s. In (b), the blue dots for the SSP5–8.5 scenario indicate the on-shelf heat transport during 2098–2100 (only shown if it exceeds the 2090s average).

only being slightly delayed beyond the year 2100. In contrast, for an atmospheric warming of  $2^\circ$  and  $3^\circ\text{C}$  in the Weddell Sea region, the lowest-emission scenario SSP1–2.6 stands out with lower on-shelf heat transport and bottom warming at Filchner Trough than for the same atmospheric warming in the other three scenarios. Separating the SSP1–2.6 scenario into the time before and after peak atmospheric  $\text{CO}_2$  levels are reached (2063; Fig. 2a), the projected median bottom warming for a local

atmospheric warming of  $3^\circ\text{C}$  is lower after ( $0.026^\circ\text{C}$ ) than before the peak ( $0.035^\circ\text{C}$ ; not shown). Altogether, this suggests that the southern Weddell Sea shelf might retain its dense-shelf characteristics well beyond the year 2100 for this scenario.

#### 4. Discussion

Based on the projected accelerating changes in shelf–open-ocean coupling and in water-mass properties on the continental shelves, our results show that by the year 2100 critical thresholds have been crossed in the southern Weddell Sea for the highest-emission scenario SSP5–8.5, but not (yet) for the three lower-emission scenarios. As a result, in the SSP5–8.5 scenario, the southern Weddell Sea switches from a *dense shelf* in the present-day to a regime resembling a *warm shelf* toward the end of the twenty-first century, with the changes being most pronounced in the vicinity of Filchner Trough after 2080. In particular, this system change is apparent through 1) the reduced potential of newly formed dense waters to reach the abyss (Fig. 5), 2) the associated reduction in carbon sequestration (Fig. 2), 3) the accelerated property-changes of bottom waters on the continental shelves (Figs. 6 and 7), and 4) the sudden increase in on-shelf heat transport in the last few years of the simulation (Fig. 9). In our model, the erosion of density differences between waters on the continental shelves and in the open ocean, which is driven by a freshening on the shelves (not shown), weakens the ASF over time and eventually facilitates the continuous flushing of the Filchner Trough with WDW, although a high-density bias in the WDW core offshore possibly leads to an earlier flushing than expected otherwise (Nissen et al. 2022). Even if, due to its timing, the full impact of this system change is not realized by the end of our model experiment, ice-shelf basal melt rates already accelerate at the very end of the simulation (59% of the increase between the 1990s and 2090s occurs in the 2090s; Nissen et al. 2022) and can be expected to accelerate further after the year 2100, as WDW further invades the ice-shelf cavity (Hellmer et al. 2012, 2017; Naughten et al. 2021; Haid et al. 2022). Consequently, a self-sustaining positive feedback will be set in motion: The enhanced freshwater input makes waters on the continental shelves even lighter, allowing for further on-shelf flow of WDW, and further stabilizing the system in its new warm state. Thereby, our findings support the tipping-point cascade proposed by Hellmer et al. (2017). Based on our results, we here suggest extending the cascade by biogeochemical elements, namely the reduction in carbon and oxygen transport to the abyss with newly formed dense waters and the reduction in oxygen and pH levels on the continental shelves. It should be noted that any global, climate-relevant impacts of reductions in the Weddell Sea deep-ocean transfer of carbon with newly formed dense waters will take up to millennia to unfold (Marinov et al. 2006). Due to computational constraints, their magnitude can thus not be quantified with our model setup. Additionally, the response of other dense-shelf regions such as the Ross Sea to the projected climate change needs to be quantified concurrently. In contrast, the projected changes in water-mass properties on the Weddell Sea continental shelves and slopes following the regime shift (i.e., warming, freshening, deoxygenation, and acidification) are expected to impact ice-sheet

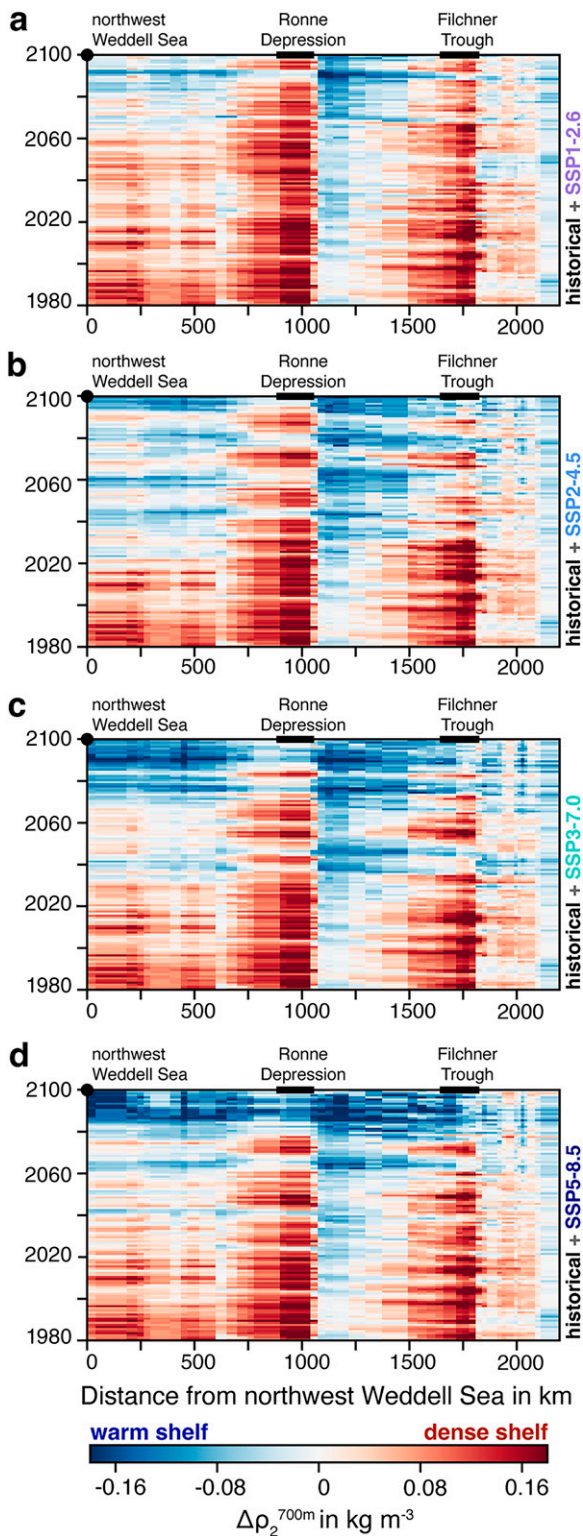


FIG. 10. Temporal evolution of the cross-shelf break density difference at 700 m from the northwestern Weddell Sea to the Filchner Trough (density at the continental shelf break minus density in the open ocean; see Eq. (2); see Fig. 1a for the start and end point of the transect). The term  $\rho_2$ , i.e., the potential

stability, global sea level rise, and ecosystems on a much shorter time scale.

Understanding the factors controlling the cross-shelf-break exchange in the southern Weddell Sea is crucial to establish (measurable) early warning indicators for the onset of this physical and biogeochemical tipping point cascade. As demonstrated by the close agreement on decadal and multidecadal time scales (Fig. 11), the erosion of density gradients due to freshening and warming of shelf waters appears to be a key ingredient for the enhancement of the on-shelf WDW transport, in agreement with observations and modeling results by Daae et al. (2020), Bull et al. (2021), and Haid et al. (2022). In our simulation, the high interannual variability in on-shelf heat transport reveals that density differences are not the only controlling factor, with negative density gradients not immediately causing enhanced on-shelf transport. Acknowledging the difficulty to fully disentangle the different contributing factors to changes in cross-shelf-break exchange in our future scenarios under shared socioeconomic pathways, this finding agrees with the idealized modeling experiments by Daae et al. (2020), in which both freshening of shelf waters and a lifting of the open-ocean thermocline were needed to induce enhanced on-shelf heat transport. As a direct consequence of wind-driven changes in Weddell Gyre circulation, which intensifies and moves closer to the shelf break (Nissen et al. 2022), the WDW overall shifts southward by 2100 in our experiments, explaining why the strongest bottom warming and deoxygenation occur along the continental slope (Fig. 3). Consequently, the WDW is lifted as well, contributing to eventually pushing the WDW onto the continental shelves (see also, e.g., Hellmer et al. 2017; Daae et al. 2020). Likewise, a southward shift of WDW is also plausible in response to an overall reduction in the volume of dense bottom waters in the open ocean as newly formed dense waters become lighter (Li et al. 2023), and dedicated sensitivity experiments would be needed to fully disentangle the relative importance of the factors controlling the regime shift in our model. An analysis of daily averaged velocity and temperature fields for the SSP5–8.5 scenario suggests that the projected twenty-first-century change in eddy kinetic energy (Fig. S1 in the online supplemental material) and the eddy-induced heat transport at Filchner Trough (Fig. 9) do not substantially affect our conclusions drawn from monthly model output throughout this paper. Yet, the eddy-induced contribution to the total on-shelf heat transport amounts to 19% below 400 m in the 1990s, implying pronounced submonthly variability that should be assessed in future work. Today, a flow of modified WDW

density referenced to 2000 dbar (in  $\text{kg m}^{-3}$ ), is calculated at 700 m, i.e., at the bottom of the shelf break and within the WDW core offshore (Nissen et al. 2022). Here, “open ocean” is defined as locations with a water depth  $\geq 2000$  m (see section 2). Results are shown for the historical period from 1980 to 2014 and for the four emission scenarios thereafter in the different panels. Red colors denote regions where the density at the continental shelf break exceeds that in the open ocean, which characterizes a “dense shelf” (Thompson et al. 2018).

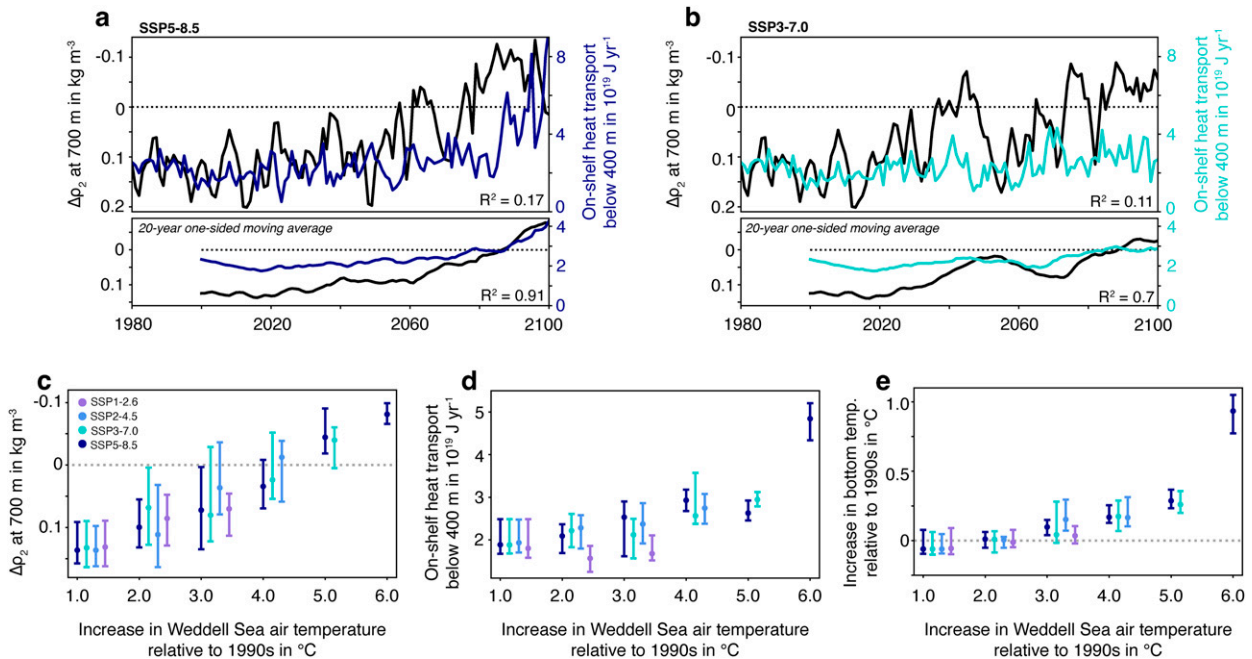


FIG. 11. (a),(b) (top) Time series of the cross-shelf break density difference at 700 m [ $\text{in kg m}^{-3}$ ; black; left y axis; density at the continental shelf break minus density in the open ocean; see Eq. (2); note that the y axis has positive values at the lower end] and the on-shelf heat transport below 400 m ( $\text{in } 10^{19} \text{ J yr}^{-1}$ ; colors; right y axis; see also Figs. 9 and 10) at Filchner Trough for the (a) SSP5–8.5 and (b) SSP3–7.0 scenario. (a),(b) (bottom) The 20-yr one-sided moving averages of the time series, and squared correlation coefficients ( $R^2$ ) are given in the lower-right corner. (c) Median potential density difference (see also Fig. 10; note the y axis), (d) median on-shelf heat transport below 400 m (see also Fig. 9), and (e) median increase in bottom temperatures ( $\text{in } ^\circ\text{C}$ ; see also Fig. 8) at the continental shelf break at Filchner Trough binned as a function of the increase in Weddell Sea air temperature relative to the 1990s. Whiskers denote the 10th and 90th percentiles, and colors show the different emission scenarios.

onto the continental shelf and into Filchner Trough is observed as part of a seasonal signal (Ryan et al. 2017) that is subject to strong interannual variability (Árthun et al. 2012) and assessing the future changes in the seasonality and frequency of occurrence could shed further light on the mechanisms at work.

To some extent, our results can be used to inform society on the potential avoidability of a regime shift in the southern Weddell Sea under climate-mitigation scenarios. For the SSP3–7.0, SSP2–4.5, and SSP1–2.6 scenarios, the system change has not yet taken place by the year 2100, and the subsurface on-shelf transport of warm, oxygen-poor WDW is not yet substantially enhanced (Fig. 9). However, conditions similar to those in the present day are preserved only for the SSP1–2.6 scenario, which is the only tested scenario in which peak atmospheric  $\text{CO}_2$  levels are reached midcentury. There are indications that the transitioning to a different regime has started for the SSP3–7.0 and SSP2–4.5 scenarios (see carbon sequestration and density gradients; Figs. 2 and 10), suggesting that an abrupt increase in on-shelf WDW transport might be imminent. While this implies little or no avoidability of the regime shift soon after the year 2100 especially for the SSP3–7.0 scenario, we note that it remains unclear whether the system change in these higher-emission scenarios could still be averted if atmospheric  $\text{CO}_2$  levels declined after 2100. The imminent system change is further supported by the similarity of projected oceanic change for scenarios SSP5–8.5 and SSP3–7.0 when compared to the

projected local atmospheric warming (Fig. 11). In addition, for the SSP3–7.0 scenario, pulses of WDW at the continental shelf break become more frequent during 2080–2100, which is similar to during 2060–80 for the SSP5–8.5 scenario, that is, just prior to the drastic increase in on-shelf heat transport (Fig. 8). Based on this observation, a systematic statistical analysis of these WDW pulses at the continental shelf break may well reveal a possible early warning indicator of the changing system (Lenton et al. 2012; Rosier et al. 2021).

The regions of the largest projected warming, deoxygenation, and acidification (i.e., the southern Weddell Sea continental shelves and particularly the Filchner Trough region and the continental slope; Fig. 3) host a variety of keystone fish species, whose life cycles critically depend on local temperatures, pH, oxygen levels, sea ice conditions, and circulation (e.g., Antarctic toothfish/*Dissostichus mawsoni*, icefish/*Neopagetopsis ionah*, or Antarctic silverfish/*Pleuragramma antarctica*; see Teschke et al. 2019; Caccavo et al. 2019; Purser et al. 2022). In our model experiments, the projected decadal average bottom oxygen concentrations for the 2090s are still well above hypoxic or anoxic oxygen concentrations even in the highest-emission scenario. Noting that a new steady state has not been reached yet and that property changes accelerate toward the end of the highest-emission scenario (Fig. 6), whether or not the projected decline of  $>100 \text{ mmol m}^{-3}$  in oxygen and the warming of  $>1^\circ\text{C}$  is already sufficient to reduce the habitat for benthic ecosystems

and local fish species should be assessed with the metabolic index (Deutsch et al. 2015) or the aerobic growth index (Clarke et al. 2021), which quantify the combined impact of warming and deoxygenation for any given species. Further, although not directly assessed in this study, changes in the circulation on the southern continental shelves, particularly the increase in on-shelf transport at a concurrent reduction in off-shelf transport [see also discussion in Hellmer et al. (2012, 2017)], might directly negatively impact the recruitment of, e.g., Antarctic silverfish (Caccavo et al. 2019). Similarly, ocean acidification has been shown to negatively impact the development stages of Antarctic fish (Flynn et al. 2015; Davis et al. 2018), although the limited number of available studies has to be acknowledged (Hancock et al. 2020). Therefore, given these potential ecological impacts resulting from the changes in the physical–biogeochemical environment, a system change in the southern Weddell Sea should be avoided.

Altogether, our results demonstrate that the interplay of local changes on the continental shelves and remote changes in the wider region ultimately controls the crossing of critical thresholds and the subsequent regime shift in the southern Weddell Sea. Different time scales are associated with how quickly 1) ecosystems on the continental shelf and along the slope are affected by changes in water-mass properties (immediate), 2) the enhanced on-shelf flow of WDW translates into enhanced ice-shelf basal melt and ultimately ice-sheet instability (decades and more), 3) deep-ocean oxygen is affected by the reduced ocean ventilation (decades and more), and 4) a reduced deep-ocean transfer of newly formed dense shelf water impacts global ocean circulation and climate (centuries to millennia). As a result, while the regime shift identified here involves the crossing of a tipping point in its generic definition (i.e., a rapid system change into a qualitatively different state that is outside its previous seasonal and interannual variability) (Figs. 2, 6, 7, and 10 herein; see Heinze et al. 2021), it remains less obvious whether it is equivalent to the crossing of a climatically relevant tipping point in the sense of Lenton et al. (2008, 2019), and Pörtner et al. (2019) because the full impact of the regional regime shift has not unfolded yet by the end of our simulations. Nonetheless, the property changes of local water masses resulting from the regime shift will ultimately impact regions downstream of the Weddell Sea given its connectivity to all major ocean basins, impacting ocean circulation, climate, and ecosystems globally.

## 5. Conclusions

Using projections with a global ocean–biogeochemistry model forced under four emission scenarios for the twenty-first century, we present multiple lines of evidence that a regime shift has taken place by 2100 for the high-emission scenario SSP5–8.5, but not (yet) for the three lower-emission scenarios. Assessing the evolution of shelf–open-ocean density gradients, time series characteristics of bottom-water properties, and the on-shelf transport of Warm Deep Water, our findings indicate that by 2100, the southern Weddell Sea has converted into a *warm shelf* regime for the SSP5–8.5 scenario and will likely do so soon after for the high and intermediate scenarios SSP3–7.0 and SSP2–4.5. As this regime shift has large implications for 1) ocean circulation and

climate (on up to millennial time scales; via a reduction of dense-water formation and heat and carbon transfer to the abyss and deep ocean ventilation), 2) global sea level (decadal and more; due to the destabilization and imminent disintegration of the West Antarctic Ice Sheet), and 3) ecosystems (immediate; due to ocean acidification, via the flushing of the continental shelves with warm, oxygen-poor waters), continued monitoring is necessary to work toward identifying early warning indicators of this system change. Our results project the largest changes in the Filchner Trough region, and changes in the frequency, duration, and magnitude of pulses of onshore transport of warm, oxygen-poor waters might serve as such an indicator. Altogether, given that the regime shift is only avoidable for the SSP1–2.6 scenario in our model experiments, for which the warming of global air temperatures is projected to remain below 2°C relative to preindustrial conditions in the AWI Climate Model forcing used here (Semmler et al. 2020), strong mitigation efforts are necessary to avoid crossing critical thresholds in this key region.

*Acknowledgments.* This project has received funding from the European Union's Horizon 2020 research and innovation programme under Grant Agreement 820989 (project COMFORT), from the Initiative and Networking Fund of the Helmholtz Association [Helmholtz Young Investigator Group *Marine Carbon and Ecosystem Feedbacks in the Earth System (MarESys)*, Grant VH-NG-1301], and from the Helmholtz Climate Initiative REKLIM (Regional Climate Change), a joint research project of the Helmholtz Association of German Research Centres (HGF). The work reflects only the authors' view; the European Commission and their executive agency are not responsible for any use that may be made of the information the work contains. Computing resources were provided by the North-German Supercomputing Alliance (HLRN) project hbk00079.

*Data availability statement.* The model data underlying the analysis in this paper are deposited at <https://doi.org/10.5281/zenodo.8029927> (Nissen et al. 2023). Additional model output and analysis scripts will be made available upon request to the corresponding author.

## REFERENCES

- Akaike, H., 1974: A new look at the statistical model identification. *IEEE Trans. Autom. Control*, **19**, 716–723, <https://doi.org/10.1109/TAC.1974.1100705>.
- Akhoudas, C. H., and Coauthors, 2021: Ventilation of the abyss in the Atlantic sector of the Southern Ocean. *Sci. Rep.*, **11**, 6760, <https://doi.org/10.1038/s41598-021-86043-2>.
- Årthun, M., K. W. Nicholls, K. Makinson, M. A. Fedak, and L. Boehme, 2012: Seasonal inflow of warm water onto the southern Weddell Sea continental shelf, Antarctica. *Geophys. Res. Lett.*, **39**, L17601, <https://doi.org/10.1029/2012GL052856>.
- Bamber, J. L., R. E. M. Riva, B. L. A. Vermeersen, and A. M. LeBrocq, 2009: Reassessment of the potential sea-level rise from a collapse of the West Antarctic ice sheet. *Science*, **324**, 901–903, <https://doi.org/10.1126/science.1169335>.
- Beaulieu, C., and R. Killick, 2018: Distinguishing trends and shifts from memory in climate data. *J. Climate*, **31**, 9519–9543, <https://doi.org/10.1175/JCLI-D-17-0863.1>.



- Bull, C. Y. S., A. Jenkins, N. C. Jourdain, I. Vaňková, P. R. Holland, P. Mathiot, U. Hausmann, and J.-B. Sallée, 2021: Remote control of Filchner-Ronne ice shelf melt rates by the Antarctic Slope Current. *J. Geophys. Res. Oceans*, **126**, e2020JC016550, <https://doi.org/10.1029/2020JC016550>.
- Caccavo, J. A., J. R. Ashford, S. Ryan, C. Papetti, M. Schröder, and L. Zane, 2019: Spatial structuring and life history connectivity of Antarctic silverfish along the southern continental shelf of the Weddell Sea. *Mar. Ecol. Prog. Ser.*, **624**, 195–212, <https://doi.org/10.3354/meps13017>.
- Clarke, T. M., C. C. C. Wabnitz, S. Striegel, T. L. Frölicher, G. Reygondeau, and W. W. L. Cheung, 2021: Aerobic growth index (AGI): An index to understand the impacts of ocean warming and deoxygenation on global marine fisheries resources. *Prog. Oceanogr.*, **195**, 102588, <https://doi.org/10.1016/j.pocean.2021.102588>.
- Daae, K., T. Hattermann, E. Darelus, R. D. Mueller, K. A. Naughten, R. Timmermann, and H. H. Hellmer, 2020: Necessary conditions for warm inflow toward the Filchner Ice Shelf, Weddell Sea. *Geophys. Res. Lett.*, **47**, e2020GL089237, <https://doi.org/10.1029/2020GL089237>.
- Danilov, S., Q. Wang, R. Timmermann, N. Iakovlev, D. Sidorenko, M. Kimmritz, T. Jung, and J. Schröder, 2015: Finite-Element Sea Ice Model (FESIM), version 2. *Geosci. Model Dev.*, **8**, 1747–1761, <https://doi.org/10.5194/gmd-8-1747-2015>.
- Darelus, E., and J. B. Sallée, 2018: Seasonal outflow of ice shelf water across the front of the Filchner Ice Shelf, Weddell Sea, Antarctica. *Geophys. Res. Lett.*, **45**, 3577–3585, <https://doi.org/10.1002/2017GL076320>.
- , I. Fer, and K. W. Nicholls, 2016: Observed vulnerability of Filchner-Ronne Ice Shelf to wind-driven inflow of warm deep water. *Nat. Commun.*, **7**, 12300, <https://doi.org/10.1038/ncomms12300>.
- Davis, B. E., E. E. Flynn, N. A. Miller, F. A. Nelson, N. A. Fangue, and A. E. Todgham, 2018: Antarctic emerald rockcod have the capacity to compensate for warming when uncoupled from CO<sub>2</sub>-acidification. *Global Change Biol.*, **24**, e655–e670, <https://doi.org/10.1111/gcb.13987>.
- Deutsch, C., A. Ferrel, B. Seibel, H.-O. Pörtner, and R. B. Huey, 2015: Climate change tightens a metabolic constraint on marine habitats. *Science*, **348**, 1132–1135, <https://doi.org/10.1126/science.aaa1605>.
- Fahrbach, E., G. Rohardt, M. Schröder, and V. Strass, 1994: Transport and structure of the Weddell Gyre. *Ann. Geophys.*, **12**, 840–855, <https://doi.org/10.1007/s00585-994-0840-7>.
- Flynn, E. E., B. E. Bjelde, N. A. Miller, and A. E. Todgham, 2015: Ocean acidification exerts negative effects during warming conditions in a developing Antarctic fish. *Conserv. Physiol.*, **3**, cov033, <https://doi.org/10.1093/conphys/cov033>.
- Foldvik, A., T. Gammelsrød, and T. Tørresen, 1985: Circulation and water masses on the southern Weddell Sea shelf. *Oceanology of the Antarctic Continental Shelf*, S. S. Jacobs, Ed., Antarctic Research Series, Vol. 43, Amer. Geophys. Union, 5–20.
- Frölicher, T. L., M. T. Aschwanen, N. Gruber, S. L. Jaccard, J. P. Dunne, and D. Paynter, 2020: Contrasting upper and deep ocean oxygen response to protracted global warming. *Global Biogeochem. Cycles*, **34**, e2020GB006601, <https://doi.org/10.1029/2020GB006601>.
- Gordon, A., 2001: Bottom water formation. *Encyclopedia of Ocean Sciences*, Academic Press, 334–340, <https://doi.org/10.1006/rwos.2001.0006>.
- Haid, V., R. Timmermann, O. Gürses, and H. H. Hellmer, 2022: On the drivers of regime shifts in the Antarctic marginal seas. *EGU-sphere*, <https://doi.org/10.5194/egusphere-2022-1044>, in press.
- Hancock, A. M., C. K. King, J. S. Stark, A. McMin, and A. T. Davidson, 2020: Effects of ocean acidification on Antarctic marine organisms: A meta-analysis. *Ecol. Evol.*, **10**, 4495–4514, <https://doi.org/10.1002/ece3.6205>.
- Hauck, J., C. Völker, T. Wang, M. Hoppema, M. Losch, and D. A. Wolf-Gladrow, 2013: Seasonally different carbon flux changes in the Southern Ocean in response to the Southern Annular Mode. *Global Biogeochem. Cycles*, **27**, 1236–1245, <https://doi.org/10.1002/2013GB004600>.
- Heinze, C., and Coauthors, 2021: The quiet crossing of ocean tipping points. *Proc. Natl. Acad. Sci. USA*, **118**, e2008478118, <https://doi.org/10.1073/pnas.2008478118>.
- Hellmer, H. H., F. Kauker, R. Timmermann, J. Determann, and J. Rae, 2012: Twenty-first-century warming of a large Antarctic ice-shelf cavity by a redirected coastal current. *Nature*, **485**, 225–228, <https://doi.org/10.1038/nature11064>.
- , —, —, and T. Hattermann, 2017: The fate of the southern Weddell Sea continental shelf in a warming climate. *J. Climate*, **30**, 4337–4350, <https://doi.org/10.1175/JCLI-D-16-0420.1>.
- Holland, P. R., T. J. Bracegirdle, P. Dutrieux, A. Jenkins, and E. J. Steig, 2019: West Antarctic ice loss influenced by internal climate variability and anthropogenic forcing. *Nat. Geosci.*, **12**, 718–724, <https://doi.org/10.1038/s41561-019-0420-9>.
- Hoppema, M., 2004: Weddell Sea is a globally significant contributor to deep-sea sequestration of natural carbon dioxide. *Deep-Sea Res. I*, **51**, 1169–1177, <https://doi.org/10.1016/j.dsr.2004.02.011>.
- , O. Klatt, W. Roether, E. Fahrbach, K. Bulsiewicz, C. Rodehacke, and G. Rohardt, 2001: Prominent renewal of Weddell Sea deep water from a remote source. *J. Mar. Res.*, **59**, 257–279, <https://doi.org/10.1357/002224001762882655>.
- Huhn, O., M. Rhein, M. Hoppema, and S. van Heuven, 2013: Decline of deep and bottom water ventilation and slowing down of anthropogenic carbon storage in the Weddell Sea, 1984–2011. *Deep-Sea Res. I*, **76**, 66–84, <https://doi.org/10.1016/j.dsr.2013.01.005>.
- Jacobs, S. S., 1991: On the nature and significance of the Antarctic slope front. *Mar. Chem.*, **35**, 9–24, [https://doi.org/10.1016/S0304-4203\(09\)90005-6](https://doi.org/10.1016/S0304-4203(09)90005-6).
- , 2004: Bottom water production and its links with the thermohaline circulation. *Antarct. Sci.*, **16**, 427–437, <https://doi.org/10.1017/S095410200400224X>.
- Janout, M. A., and Coauthors, 2021: FRIS revisited in 2018: On the circulation and water masses at the Filchner and Ronne ice shelves in the southern Weddell Sea. *J. Geophys. Res. Oceans*, **126**, e2021JC017269, <https://doi.org/10.1029/2021JC017269>.
- Karakaş, O., C. Völker, M. Iversen, W. Hagen, D. Wolf-Gladrow, B. Fach, and J. Hauck, 2021: Modeling the impact of macrozooplankton on carbon export production in the Southern Ocean. *J. Geophys. Res. Oceans*, **126**, e2021JC017315, <https://doi.org/10.1029/2021JC017315>.
- Killick, R., C. Beaulieu, S. Taylor, and H. Hullait, 2021: EnvCpt: Detection of structural changes in climate and environment time series, version 1.1.3. R package, <https://github.com/rkillick/EnvCpt/>.
- Lenton, T. M., H. Held, E. Kriegler, J. W. Hall, W. Lucht, S. Rahmstorf, and H. J. Schellnhuber, 2008: Tipping elements in the Earth's climate system. *Proc. Natl. Acad. Sci. USA*, **105**, 1786–1793, <https://doi.org/10.1073/pnas.0705414105>.
- , V. N. Livina, V. Dakos, E. H. van Nes, and M. Scheffer, 2012: Early warning of climate tipping points from critical slowing down: Comparing methods to improve robustness. *Philos. Trans. Roy. Soc.*, **370A**, 1185–1204, <http://www.jstor.org/stable/41348438>.

- , J. Rockström, O. Gaffney, S. Rahmstorf, K. Richardson, W. Steffen, and H. J. Schellnhuber, 2019: Climate tipping points—Too risky to bet against. *Nature*, **575**, 592–595, <https://doi.org/10.1038/d41586-019-03595-0>.
- Li, Q., M. H. England, A. M. Hogg, S. R. Rintoul, and A. K. Morrison, 2023: Abyssal ocean overturning slowdown and warming driven by Antarctic meltwater. *Nature*, **615**, 841–847, <https://doi.org/10.1038/s41586-023-05762-w>.
- Lockwood, J. W., C. O. Dufour, S. M. Griffies, and M. Winton, 2021: On the role of the Antarctic slope front on the occurrence of the Weddell Sea Polynya under climate change. *J. Climate*, **34**, 2529–2548, <https://doi.org/10.1175/JCLI-D-20-0069.1>.
- Marinov, I., A. Gnanadesikan, J. R. Toggweiler, and J. L. Sarmiento, 2006: The Southern Ocean biogeochemical divide. *Nature*, **441**, 964–967, <https://doi.org/10.1038/nature04883>.
- Matear, R. J., A. C. Hirst, and B. I. McNeil, 2000: Changes in dissolved oxygen in the Southern Ocean with climate change. *Geochim. Geophys. Geosyst.*, **1**, 1050, <https://doi.org/10.1029/2000GC000086>.
- Meinshausen, M., and Coauthors, 2017: Historical greenhouse gas concentrations for climate modelling (CMIP6). *Geosci. Model Dev.*, **10**, 2057–2116, <https://doi.org/10.5194/gmd-10-2057-2017>.
- Mercer, J. H., 1968: Antarctic ice and Sangamon sea level. *IAHS Publ.*, **179**, 217–225, <https://iahs.info/uploads/dms/079020.pdf>.
- , 1978: West Antarctic ice sheet and CO<sub>2</sub> greenhouse effect: A threat of disaster. *Nature*, **271**, 321–325, <https://doi.org/10.1038/271321a0>.
- Meredith, M. P., 2013: Replenishing the abyss. *Nat. Geosci.*, **6**, 166–167, <https://doi.org/10.1038/ngeo1743>.
- Morrison, A. K., A. M. Hogg, M. H. England, and P. Spence, 2020: Warm circumpolar deep water transport toward Antarctica driven by local dense water export in canyons. *Sci. Adv.*, **6**, eaav2516, <https://doi.org/10.1126/sciadv.aav2516>.
- Naughten, K. A., A. Jenkins, P. R. Holland, R. I. Muford, K. W. Nicholls, and D. R. Munday, 2019: Modeling the influence of the Weddell Polynya on the Filchner–Ronne ice shelf cavity. *J. Climate*, **32**, 5289–5303, <https://doi.org/10.1175/JCLI-D-19-0203.1>.
- , J. De Rydt, S. H. R. Rosier, A. Jenkins, P. R. Holland, and J. K. Ridley, 2021: Two-timescale response of a large Antarctic ice shelf to climate change. *Nat. Commun.*, **12**, 1991, <https://doi.org/10.1038/s41467-021-22259-0>.
- Nissen, C., R. Timmermann, M. Hoppema, Ö. Gürses, and J. Hauck, 2022: Abruptly attenuated carbon sequestration with Weddell Sea dense waters by 2100. *Nat. Commun.*, **13**, 3402, <https://doi.org/10.1038/s41467-022-30671-3>.
- , —, —, and J. Hauck, 2023: FESOM-REcoM model data: A regime shift on Weddell Sea continental shelves with local and remote physical-biogeochemical implications is avoidable in a 2°C scenario [dataset]. Zenodo, last accessed August 2023, <https://doi.org/10.5281/zenodo.8029927>.
- O'Neill, B. C., and Coauthors, 2016: The Scenario Model Inter-comparison Project (ScenarioMIP) for CMIP6. *Geosci. Model Dev.*, **9**, 3461–3482, <https://doi.org/10.5194/gmd-9-3461-2016>.
- Oppenheimer, M., 1998: Global warming and the stability of the West Antarctic ice sheet. *Nature*, **393**, 325–332, <https://doi.org/10.1038/30661>.
- Orr, J. C., and J.-M. Epitalon, 2015: Improved routines to model the ocean carbonate system: mocsy 2.0. *Geosci. Model Dev.*, **8**, 485–499, <https://doi.org/10.5194/gmd-8-485-2015>.
- Pörtner, H.-O., and Coauthors, Eds., 2019: *The Ocean and Cryosphere in a Changing Climate*. Cambridge University Press, 755 pp.
- Purser, A., and Coauthors, 2022: A vast icefish breeding colony discovered in the Antarctic. *Curr. Biol.*, **32**, 842–850, <https://doi.org/10.1016/j.cub.2021.12.022>.
- Rignot, E., S. Jacobs, J. Mouginot, and B. Scheuchl, 2013: Ice-shelf melting around Antarctica. *Science*, **341**, 266–270, <https://doi.org/10.1126/science.1235798>.
- , J. Mouginot, B. Scheuchl, M. van den Broeke, M. J. van Wessem, and M. Morlighem, 2019: Four decades of Antarctic Ice Sheet mass balance from 1979–2017. *Proc. Natl. Acad. Sci. USA*, **116**, 1095–1103, <https://doi.org/10.1073/pnas.1812883116>.
- Rocha, J. C., G. Peterson, Ö. Bodin, and S. Levin, 2018: Cascading regime shifts within and across scales. *Science*, **362**, 1379–1383, <https://doi.org/10.1126/science.aat7850>.
- Rosier, S. H. R., R. Reese, J. F. Donges, J. De Rydt, G. H. Gudmundsson, and R. Winkelmann, 2021: The tipping points and early warning indicators for Pine Island Glacier, West Antarctica. *Cryosphere*, **15**, 1501–1516, <https://doi.org/10.5194/tc-15-1501-2021>.
- Ryan, S., T. Hattermann, E. Darelius, and M. Schröder, 2017: Seasonal cycle of hydrography on the eastern shelf of the Filchner Trough, Weddell Sea, Antarctica. *J. Geophys. Res. Oceans*, **122**, 6437–6453, <https://doi.org/10.1002/2017JC012916>.
- , H. H. Hellmer, M. Janout, E. Darelius, L. Vignes, and M. Schröder, 2020: Exceptionally warm and prolonged flow of warm deep water toward the Filchner–Ronne ice shelf in 2017. *Geophys. Res. Lett.*, **47**, e2020GL088119, <https://doi.org/10.1029/2020GL088119>.
- Scheffer, M., S. Carpenter, J. A. Foley, C. Folke, and B. Walker, 2001: Catastrophic shifts in ecosystems. *Nature*, **413**, 591–596, <https://doi.org/10.1038/35098000>.
- Semmler, T., and Coauthors, 2020: Simulations for CMIP6 with the AWI Climate Model AWI-CM-1-1. *J. Adv. Model. Earth Syst.*, **12**, e2019MS002009, <https://doi.org/10.1029/2019MS002009>.
- Teschke, K., H. Pehlke, and T. Brey, 2019: Spatial distribution of demersal and pelagic fishes in the wider Weddell Sea (Antarctica) with links to ArcGIS map packages. PANGAEA, accessed 21 November 2022, <https://doi.org/10.1594/PANGAEA.899591>.
- Thompson, A. F., A. L. Stewart, P. Spence, and K. J. Heywood, 2018: The Antarctic slope current in a changing climate. *Rev. Geophys.*, **56**, 741–770, <https://doi.org/10.1029/2018RG000624>.
- Timmermann, R., and H. H. Hellmer, 2013: Southern Ocean warming and increased ice shelf basal melting in the twenty-first and twenty-second centuries based on coupled ice-ocean finite-element modelling. *Ocean Dyn.*, **63**, 1011–1026, <https://doi.org/10.1007/s10236-013-0642-0>.
- , and S. Goeller, 2017: Response to Filchner–Ronne Ice Shelf cavity warming in a coupled ocean–ice sheet model—Part 1: The ocean perspective. *Ocean Sci.*, **13**, 765–776, <https://doi.org/10.5194/os-13-765-2017>.
- , Q. Wang, and H. Hellmer, 2012: Ice-shelf basal melting in a global finite-element sea-ice/ice-shelf/ocean model. *Ann. Glaciol.*, **53**, 303–314, <https://doi.org/10.3189/2012AOG60A156>.
- van Heuven, S. M. A. C., M. Hoppema, E. M. Jones, and H. J. W. de Baar, 2014: Rapid invasion of anthropogenic CO<sub>2</sub> into the deep circulation of the Weddell Gyre. *Philos. Trans. Roy. Soc.*, **372A**, 20130056, <https://doi.org/10.1098/rsta.2013.0056>.
- Vernet, M., and Coauthors, 2019: The Weddell Gyre, Southern Ocean: Present knowledge and future challenges. *Rev. Geophys.*, **57**, 623–708, <https://doi.org/10.1029/2018RG000604>.
- Wang, Q., S. Danilov, D. Sidorenko, R. Timmermann, C. Wekerle, X. Wang, T. Jung, and J. Schröter, 2014: The Finite Element Sea Ice–Ocean Model (FESOM) v.1.4: Formulation of an ocean general circulation model. *Geosci. Model Dev.*, **7**, 663–693, <https://doi.org/10.5194/gmd-7-663-2014>.